The differential virulence of Fusarium strains causing corneal infections and plant diseases is associated with accessory chromosome composition

Dilay Hazal Ayhan[1,2], Serena Abbondante[3], Domingo Martínez-Soto[4], Shira Milo[1], Katherine Rickelton[1,2], Vista Sohrab[1‡], Shunsuke Kotera[5], Tsutomu Arie[5], Michaela Ellen Marshall[3], Marina Campos Rocha[6], Sajeet Haridas[7], Igor V. Grigoriev[7], Neta Shlezinger[6], Eric Pearlman[3], Li-Jun Ma [1,2 #]

[1] Biochemistry and Molecular Biology, [2] Molecular and Cellular Biology, University of Massachusetts Amherst, Amherst, MA, USA

[3] Physiology and Biophysics and Ophthalmology, University of California, Irvine, USA

University of Massachusetts Amherst, Amherst, MA, USA

[4] Department of Microbiology, Centro de Investigación Científica y Educación Superior de Ensenada (CICESE), Ensenada, Baja California, Mexico.

[5] Laboratory of Plant Pathology, Graduate School of Agriculture, Tokyo University of Agriculture and Technology (TUAT), Fuchu, Tokyo, Japan

[6] The Robert H. Smith Faculty of Agriculture, Food and Environment, The Hebrew University of Jerusalem, Jerusalem, Israel

[7] US Department of Energy Joint Genome Institute, Lawrence Berkeley National Laboratory, Berkeley, CA 94720, USA

*Present address: Mitsui chemicals crop & life solutions, Inc., Mobara-shi, Chiba, 297-0017, Japan

[‡] Undergraduate student.

Running head (53 out of 54 total): Accessory chromosomes in plant versus human pathogens

[#] **Address correspondence to Li-Jun Ma** (lijun@biochem.umass.edu).

Keywords

Fusarium oxysporum, cross-kingdom fungal pathogen, corneal infection, tomato vascular wilt, accessory chromosomes, comparative genomics

ABSTRACT (231 out of 250 words)

Fusarium oxysporum is a cross-kingdom pathogen. While some strains cause disseminated fusariosis and blinding corneal infections in humans, others are responsible for devastating vascular wilt diseases in plants. To better understand the distinct adaptations of *F. oxysporum* to animal or plant hosts, we conducted a comparative phenotypic and genetic analysis of two strains: MRL8996 (isolated from a keratitis patient) and Fol4287 (isolated from a wilted tomato [*Solanum lycopersicum*]). *In vivo* infection of mouse corneas and tomato plants revealed that, while both strains cause symptoms in both hosts, MRL8996 caused more severe corneal ulceration and perforation in mice, whereas Fol4287 induced more pronounced wilting symptoms in tomato. *In vitro* assays using abiotic stress treatments revealed that the human pathogen MRL8996 was better adapted to elevated temperatures, whereas the plant pathogen Fol4287 was more tolerant of osmotic and cell wall stresses. Both strains displayed broad resistance to antifungal treatment, with MRL8996 exhibiting the paradoxical effect of increased tolerance to higher concentrations of the antifungal caspofungin. We identified a set of accessory chromosomes (ACs) and protein-encoding genes with distinct transposon profiles and functions, respectively, between MRL8996 and Fol4287. Interestingly, ACs from both genomes also encode proteins with shared functions, such as chromatin remodeling and post-translational protein modifications. Our phenotypic assays and comparative genomics analyses lay the foundation for future studies correlating genotype with phenotype and for developing targeted antifungals for agricultural and clinical uses.

Importance (146 out of 150 words)

Fusarium oxysporum is a cross-kingdom fungal pathogen that infects both plants and animals. In addition to causing many devastating wilt diseases, this group of organisms was recently recognized by the World Health Organization as a high-priority threat to human health. Climate change has increased the risk of *Fusarium* infections, as *Fusarium* strains are highly adaptable to changing environments. Deciphering fungal adaptation mechanisms is crucial to developing appropriate control strategies. We performed a comparative analysis of *Fusarium* strains using an animal (mouse) and plant (tomato) host and *in vitro* conditions that mimic abiotic stress. We also performed comparative genomics analyses to highlight the genetic differences between human and plant pathogens and correlate their phenotypic and genotypic variations. We uncovered important functional hubs shared by plant and human pathogens, such as chromatin modification, transcriptional regulation, and signal transduction, which could be used to identify novel antifungal targets.

Main text (4,971 out of 5,000 words)

INTRODUCTION

Fusarium oxysporum, a cross-kingdom pathogen, is included in the list of health-threatening fungi by the World Health Organization (WHO) (1) and is considered to be among the top five most important plant pathogens (2). Corneal infections (keratitis) caused by *Fusarium* pathogens are an important cause of blindness worldwide, resulting in over one million new cases of blindness annually (3, 4). Indeed, *Fusarium* spp. are the most common cause of fungal keratitis in India (5, 6), China (7, 8), South Africa (9), and Brazil (10). *F. oxysporum* was also the cause of the 2005–2006 keratitis outbreak among contact lens wearers in the US and other temperate regions of the world (11, 12). As a plant pathogen, *F. oxysporum* causes devastating vascular wilt diseases in many economically important crops, including tomato (*Solanum lycopersicum*) (13), cotton (*Gossypium hirsutum*) (14, 15), and banana (*Musa* sp.) (16), and is responsible for billions of dollars in annual yield losses. Disease severity caused by this cross-kingdom pathogen is compounded by the lack of effective drugs, as only a limited number of antifungal agents are available to control eukaryotic fungal pathogens, and most *Fusarium* isolates are notorious for their broad resistance to many of these drugs (17–19).

Host-specific virulence is well recognized among plant pathogenic *F. oxysporum* isolates, as a single *F. oxysporum* species complex (FOSC) member typically infects only one or two plant species and is recognized as a *forma specialis* among plant pathogens. Within the FOSC, over 100 recognized *F. oxysporum formae speciales* infect more than 100 diverse plant hosts (20). We previously identified horizontally inherited accessory chromosomes (ACs) that lack genes associated with housekeeping functions but are enriched for genes related to fungal virulence as determinants of host-specific pathogenicity within the FOSC (21–24). Therefore,

ACs (also referred to as pathogenicity chromosomes) encode several functionally validated virulence factors toward plant hosts, such as Secreted in Xylem (*SIX*) effectors (25), transcription factors (26), and kinases (27, 28). The importance of *F. oxysporum* ACs was demonstrated by the finding that a non-pathogenic *F. oxysporum* strain became virulent upon receiving ACs from a pathogenic strain (21, 29, 30).

No specific *forma specialis* has been reported for clinical isolates of *F. oxysporum*. Conventionally, disseminated fusariosis was considered to be the result of opportunistic infection of immunocompromised patients by environmental isolates, and corneal infections were considered to arise due to the limited immune responses of the human eye. The finding that a plant pathogenic isolate was able to infect immunosuppressed mice and cause disease (31) supported this notion. However, distinct sets of ACs were reported in the genomes of two clinical FOSC strains (32) and found to lack the genomic signatures that define plant pathogenic ACs, such as the presence of *SIX* effector genes and some repeat elements commonly present upstream of these genes (33). By contrast, these two clinical isolates share AC regions that are enriched in genes encoding metal ion transporters and cation transporters (32).

Using the well-established mouse fungal keratitis (4) and the tomato vascular wilt models (25), this study compared the human pathogenic strain MRL8996 isolated from a keratitis patient and the plant pathogenic strain Fol4287 isolated from a diseased tomato to test the hypothesis that distinct ACs contribute to the unique adaptation of fungal strains to animal or plant hosts. Both strains exhibited greater virulence in their respective hosts. Although we observed cross-kingdom virulence, these interactions resulted in milder disease phenotypes. These observations were supported by *in vitro* studies showing that MRL8996 was better adapted to higher temperatures, while Fol4287 tolerated conditions imposing osmotic or cell wall stress. These

phenotypic assays revealed the unique adaptations of human and plant pathogens, providing a platform to dissect their different interactions with diverse hosts. Comparative genomics highlighted distinct genetic elements unique to each strain, offering potential testable hypotheses to correlate phenotypic to genotypic variations between a human and a plant pathogen. We also uncovered some important functional hubs used by both human and plant pathogens, such as chromatin modification, transcriptional regulation, and signal transduction, presenting some untapped antifungal targets.

RESULTS

COMPARATIVE PHENOMICS REVEALS HOST-SPECIFIC ADAPTATION

We selected two *F. oxysporum* strains, one isolated from a keratitis patient and one from a tomato plant showing wilting symptoms, as representative human and plant pathogens, respectively. The keratitis strain MRL8996 was isolated from the cornea of one of the patients in the 2005–2006 contact lens–associated keratitis outbreak cohort (34). Phylogenetically, this keratitis strain is grouped with other human pathogenic isolates (35, 36). The tomato pathogenic strain Fol4287 was originally isolated from a diseased tomato plant in Spain (37, 38) and has been adopted by the international Fusarium research community as the reference strain (21).

MRL8996 is more virulent than Fol4287 in infected mouse corneas

To identify potential differences in virulence between Fol4287 and MRL8996 during corneal infection, we performed intrastromal injections in the corneal stroma of C57BL/6 mice with 5,000 conidia from strain Fol4287 or MRL8996. After 24 h, we observed severe corneal ulceration and perforation among the MRL8996-inoculated eyes (**Fig. 1A**), showing a significantly higher clinical score (a measure of disease severity) (41) compared to Fol428-

inoculated eyes (**Fig. 1B**). We also examined fungal viability following eye infection with either fungal strain and detected significantly more colony-forming units (CFUs) among samples infected with MRL8996 compared to Fol4287 (**Fig. 1C**), indicating that the host was more efficient at containing the infection and possibly killing the Fol4287 strain compared to MRL8996.

The major cause of corneal ulceration following fungal infection is the recruitment of CD45+ myeloid cells, including neutrophils to the corneal stroma, due to the secretion of serine and matrix metalloproteinases (4). To quantify the population of immune cells involved in infection with each *F. oxysporum* strain, we dissected corneas that were infected with MRL8996 or Fol4287, digested them with collagenase, and incubated the resulting cells with antibodies against CD45 and CD11b (which recognize myeloid cells in general) and Ly6G and Ly6C (which recognize neutrophils and monocytes, respectively) (42). Consistent with the extent of corneal disease and CFU data, corneas infected with MRL8996 had a greater proportion of CD45+ myeloid cells than those infected with Fol4287 (86.6% and 75.1%, respectively) (**Fig. 1D-i**). Approximately 90% of CD45+ myeloid cells were Ly6G+ neutrophils in corneas infected with each fungal strain (**Fig. 1D-ii**). Due to the higher percentage of CD45+ myeloid cells, we observed significantly more Ly6G+/CD11b+ neutrophils in corneas infected with the keratitis strain MRL8996 compared to the plant pathogenic strain Fol4287 (**Fig. 1E**). No significant difference in the number of Ly6C+/CD11b+ monocytes was detected in corneas infected with either strain (**Fig. 1D-iii,F**).

Collectively, these findings indicate that the clinical isolate MRL8996 is more virulent than the plant pathogen Fol4287 in infected corneas.

Fol4287 is more virulent than MRL8996 in infected tomato plants

To examine the relative disease severity caused by these two *F. oxysporum* strains in plants, we inoculated tomato seedlings with either strain using a well-established wilting disease assay (43–45). Briefly, we soaked cleaned roots of tomato seedlings in a 10^6 spores/mL suspension for 45 min before gently transplanting the inoculated seedlings in sterilized soil. As a mock control, roots were incubated in sterile distilled water. We used a disease index scale from 1 to 5 to measure disease severity (46), with 1 for healthy plants; 2 for plants showing wilted leaves with chlorotic areas; 3 for plants with necrotic spots; 4 for plants with wilted leaves and whole plants showing chlorosis, areas of necrosis, and defoliation; and 5 for dead plants.

At 10 days post-inoculation (dpi), the mock-inoculated seedlings were completely healthy, with a disease index of 1. By contrast, all tomato seedlings infected with the plant pathogen Fol4287 developed severe wilt symptoms, with an average disease index of 4, with wilting leaves showings areas of chlorosis, necrosis, and plant defoliation. Although the keratitis strain MRL8996 also caused wilting symptoms, with wilting leaves with chlorotic areas, the disease symptoms were significantly less pronounced, with an average disease index of 2.5 (**Fig. 2A**,**B**, **Fig. S1**).

The distinction between these strains was even more pronounced when tracking fungal colonization by confocal microscopy after wheat germ agglutinin (WGA)-Alexa Fluor 488 (green) staining of fungal cell walls and propidium iodide staining (red) of plant cell walls (47). As reported for wilt pathogens (45), the plant pathogenic strain Fol4287 invaded the xylem tissues in both primary and lateral roots at 4 dpi (**Fig. 2C**). By contrast, the keratitis strain MRL8996 did not penetrate the xylem in either primary or lateral roots. However, MRL8996

colonized the epidermis and part of the cortex in both primary and lateral roots, with some spore germination observed inside plant cells (**Fig. 2D**).

Overall, these findings demonstrate that the plant pathogen caused significantly greater disease severity in tomato seedlings than the clinical pathogen.

MRL8996 and Fol4287 exhibit resistance to different abiotic stress conditions

To explore cross-kingdom adaptation to different environmental conditions, we exposed the two *F. oxysporum* strains to the abiotic stresses of high salinity (0.6 M NaCl), oxidative stress (1 mM H_2O_2), and cell wall stress (1 mg/mL Congo Red), as well as a temperature shift from 28°C to 34°C and a pH shift from 5.0 to 7.4. The higher temperature and pH were chosen since they reflect the conditions of the human cornea (48). We calculated the growth rates of each strain at 3 dpi under each condition as the slope of the growth curve (diameter of the colony/dpi). Notably, the keratitis strain MRL8996 formed larger colonies than the plant pathogen Fol4287 in rich and minimal media at both temperatures tested (**Fig. 3A, Table S1**, **Fig. S2A**).

To examine the adaptation of these strains to stress, we calculated the ratio of their growth rates under two different conditions. For instance, to assess adaptation to different temperatures, we calculated the ratio of the fungal growth rates between 34°C and 28°C ($GR_{34°C}/GR_{28°C}$). While both strains grew more slowly at the higher temperature, the growth rate of the plant pathogen Fol4287 was significantly slower at this temperature compared to the keratitis strain MRL8996 under all conditions tested **(Fig. 3B, C)**. At 34°C, lowering the pH from the human physiological pH (7.4) to an acidic pH (5) environment decreased the growth of the keratitis strain by 40%. Our observation that the human pathogenic strain MRL8996 was

better adapted to an elevated temperature of 34°C at pH 7.4 may reflect the adaptation of the human pathogen to the host environment.

Similarly, the plant pathogenic strain Fol4287 exhibited significantly higher tolerance to osmotic stress (0.6 M NaCl) than MRL8996 (**Fig. 3C, Fig. S2B**). Compared to growth in complete medium alone at 28°C, the growth of MRL8996 in the presence of 0.6 M NaCl decreased by 16.7% relative to the control condition, whereas the growth of strain Fol4287 increased by 22.7%, revealing a significant difference in their response to osmotic stress ($p < 10^5$). At 34°C, both strains grew better under higher salinity conditions compared to complete medium alone. While the growth of MRL8996 almost doubled (increase of 99.4%) under these conditions, the growth of Fol4287 almost tripled (increase of 187.6%), which was significantly better ($p < 10^9$). Therefore, the plant pathogenic strain Fol4287 is better adapted to higher salinity conditions than MRL8996 at both temperatures (**Fig. 3C, Fig. S2B**). Further investigation is needed to determine why the presence of 0.6 M NaCl in the medium increases fungal tolerance to high temperature.

Surprisingly, 1 mM H_2O_2 treatment (to induce oxidative stress) did not affect the growth rates of either strain at 28°C. However, the human pathogenic strain MRL8996 exhibited resistance to oxidative stress, with a 28.4% increase in growth at 34°C compared to samples grown in complete medium alone. However, cell wall stress imposed by the addition of 1 mg/mL Congo Red to the medium inhibited the growth of both strains. At 28°C, compared to growth in YPD medium alone, the growth rates of MRL8996 and Fol4287 were significantly lower (by 58.8% and 52.9%, respectively). At 34°C, the growth rate was reduced by 33.3% for MRL8996 and 43.8% for Fol4287 compared to the control.

Together, these findings indicate that the clinical isolate MRL8996 is better adapted to the physical conditions of the animal host, such as elevated temperature, whereas the plant pathogenic strain Fol4287 is more tolerant to increased salinity. Therefore, the complex, interconnected regulatory relationship between the physiological adaptation of the fungus and fungal–host interactions require further characterization.

MRL8998, but not Fol4287, exhibits tolerance to high caspofungin concentrations

Caspofungin acetate (CFA), which targets 1,3-β-glucan synthase, an enzyme responsible for the biosynthesis of one of the main components of the fungal wall, is used as an antifungal agent (49, 50). However, different fungi show diverse responses to CFA, as clinical isolates of *Candida albicans* and *Aspergillus fumigatus* are sensitive to CFA (51), whereas some less common fungal human pathogens, including *Fusarium* spp., are resistant to clinically relevant levels of CFA (52). In the current study, the keratitis strain MRL8998 exhibited enhanced tolerance to high caspofungin concentrations (**Fig. 4A**). The growth rate of the plant pathogen Fol4287 decreased from 80% to 70% with an increase in caspofungin concentration from 0.2 μg/mL to 8 μg/mL compared to growth in the absence of caspofungin. By contrast, the growth rate of the keratitis strain MRL8996 decreased to 50% under 2 μg/mL caspofungin treatment and increased to 75% under 8 μg/mL caspofungin treatment compared to the control (**Fig. 4B**). We also observed the caspofungin paradoxical effect when quantifying the time needed to reach 50% conidia germination (**Fig. 4C**). While there was no significant difference in the time needed for the plant pathogen Fol4287 to reach a 50% germination rate in the presence of caspofungin, the human keratitis strain required a significantly longer time to reach 50% gemination under 0.5 μg/mL caspofungin treatment compared to the control (no caspofungin) or 8 μg/mL caspofungin treatment.

COMPARATIVE GENOMICS REVEALS STRAIN-SPECIFIC ACCESSORY CHROMOSOMES WITH DISTINCT TRANSPOSON PROFILES

We used a contour-clamped homogeneous electric field (CHEF) gel to observe the diversity of karyotypes among *F. oxysporum* genomes and confirmed the presence of ACs in Fol4287 (21, 53), MRL8996 and NRRL 32931 (32) (**Fig. 5A**). Comparative genomics confirmed the conservation of core chromosomes (CCs) (**Fig. 5B**, and **Table S2**) and revealed three small CCs (chromosomes 11, 12, and 13) that were less conserved, with an average of 94.0% sequence identity over 35.1% coverage, supporting the three-speed evolutionary hypothesis (54). The conservation of CCs enabled us to identify ACs and sequences unique to the plant or human pathogen. As highlighted in darker blue and darker green boxes in **Fig. 5B**, the genomes of MRL8996 and Fol4287 contained 6.4 Mb and 9.8 Mb of accessory sequences corresponding to 12.8% and 18.7% of the total genome, respectively. Our comparative analysis also revealed an overall conservation of the mitochondrial genome (99.0%) and highlighted a divergent sequence around open reading frame 2285 (ORF2285) (**Fig. S3**), a known variable mitochondrial region in the genus *Fusarium* (55).

The repeat contents in the Fol4287 and MRL8996 genomes were similar, with values of 6.6% and 5.4%, respectively (**File S1 and S2**). Transposable elements (TEs), a signature of accessory sequences (56), were enriched in the ACs of both genomes (27.2% and 23.8%, respectively) (**Table S3**), but with distinct transposon profiles. In the Fol4187 genome, approximately one-third of identified TEs were type I retrotransposons, another one-third was type II DNA transposons, and the last one-third was unknown repeats. In the MRL8896 genome, more than half were identified as type I and less than 20% as type II TEs (**Fig. 5C**).

As observed in the initial study comparing *Fusarium* genomes, many class I retrotransposons are shared among Fol4287, *F. graminearum*, and *F. verticillioides* (21). Similarly, some retrotransposons, such as the long terminal repeat (LTR) transposon *Copia*, were present in both the Fol4287 and MRL8996 genomes (**Fig. 5D, Table S4**). However, some LTR elements with the highest copy numbers in MRL8996, such as several *Gypsy* elements, were not present in Fol4287. Similarly, the most abundant long interspersed nuclear element (LINE) transposon in MRL8996, the *Cnl1* CRE-type non-LTR retrotransposon, was not present in Fol4287. Of the three short interspersed nuclear element (SINE) transposon families, the *Foxy2* family was the most abundant in Fol4287, while the *Foxy5* family was the most abundant in MRL8996.

Conversely, Fol4287 contained unique class II DNA transposons (**Fig. 5D, Table S4**). Although some DNA transposons were shared between the Fol4287 and MRL8996 genomes, the Fol4287 genome contained more copies of these shared transposons and harbored many unique DNA transposon families. For instance, the most abundant DNA TE in Fol4287, *Hormin* (a miniature *Hornet* element), was absent from the MRL8996 genome. Miniature impala elements (MIMPs), which are known to be involved in phytopathogenicity (33), were not present in MRL8996. Similarly, Fol4287 contained significantly more Helitrons (57) compared to MRL8996.

There were also many unclassified repeat elements that were not shared between the Fol4287 and MRL8996 genomes (**Fig. S4**). It is important to recognize the distinction between different TE profiles, as class I and class II TEs play different roles in the genome dynamics of MRL8996 and Fol4287.

STRAIN-SPECIFIC ACCESSORY CHROMOSOMES CONTRIBUTE TO DISTINCT FUNCTIONAL ADAPTATIONS

We annotated the genome of MRL8996 using the Joint Genome Institute annotation pipeline (58) and assigned Gene Ontology (GO) terms to genes in both genomes using the Mycocosm GO annotation pipeline (**Table 1**). Among the 16,631 and 20,925 predicted protein-coding genes in the MRL8996 and Fol4287 genomes, respectively, we identified 2,017 (12.1%) and 3,890 (18.6%) genes located on their respective ACs. Approximately 46.0% and 26.9% of AC genes in the genomes of MRL8996 and Fol4287 were assigned to GO terms, respectively. Their functional enrichments (p-value $< 10^{-3}$) revealed some functional categories shared by both pathogens (**Fig. 6** category III), in addition to strain-specific functions (**Fig. 6** categories I and II, **Tables S5** and **S6**).

Functional groups enriched in both genomes due to different sets of AC genes

1) *Chromatin assembly or disassembly*. The most significantly enriched functional term in both genomes was chromatin assembly or disassembly (GO:0006333), with $p = 6 \times 10^{-12}$ for MRL8996 AC genes and $p = 7 \times 10^{-15}$ for Fol4287 AC genes. Most genes under this annotation encode CHROMO domain–containing proteins that bind to the H3K9 di/trimethyl modification on histone H3, a hallmark of heterochromatic regions (59, 60) that are typically involved in the assembly or remodeling of chromatin and associated proteins or RNAs (61). A total of 27 and 12 AC genes were annotated under this category in the Fol4287 and MRL8996 genomes, respectively. Phylogenetic analysis grouped these genes into three clades (**Fig. S5**).

The first clade, sharing homologs of CHROMO domain–containing protein 2 (Chp2) from fission yeast (*Schizosaccharomyces pombe*), comprised eight AC genes in the Fol4287 AC

(FOXG_14021, FOXG_14173, FOXG_14828, FOXG_19450, FOXG_22247, FOXG_22319, FOXG_22272, and FOXG_22398) and seven in the MRL8996 AC (343182, 342348, 342933, 222573, 530934, 452706, and 222708). The second clade contained 11 AC genes in Fol4287 and three in MRL8996. Four of the Fol4287 AC genes in this clade (FOXG_06543, FOXG_06723, FOXG_07283, and FOXG_16305) are predicted to encode homologs of putative Heterochromatin protein 1 (HP1) (A0A0C4BKY0) based on AlphaFold prediction (62). The third clade contains eight AC genes in Fol4287 and two in MRL8996, including genes encoding Zinc finger C2H2-type domain–containing proteins. Notably, Chp2 and HP1 both interact with chromatin in DNA–protein complexes and are involved in heterochromatin formation. For instance, high-affinity binding was documented between the chromoshadow domain of Chp2 and the N terminus of Mit1 (Mi2-like protein Interacting with clr Three), a subunit of the nucleosome remodeling and deacetylation complex SHREC (Snf2/Hdac Repressive Complex) from fission yeast (63). Similarly, HP1, which functions as a key regulator coordinating eukaryotic chromatin compaction and transcriptional gene silencing, binds to heterochromatin marks and recruits other factors to promote heterochromatin formation (64).

2) *Post-translational modifications.* The other significantly enriched term ($p = 1.95 \times 10^{-8}$ for MRL8996 AC genes and $p = 3 \times 10^{-13}$ for Fol4287 AC genes) was protein phosphorylation (GO:0006468), an important cellular regulatory mechanism by means of kinases. This result was expected, as we previously identified a positive correlation between the total number of protein kinases encoded in a genome and the size of the proteome of an organism (65). However, each genome has its own distinct set of encoded proteins. For instance, the major AC-enriched kinases in MRL8996 are Halotolerance protein 4-like (HAL4) serine/threonine kinases (which regulate ion transporters), Calmodulin Dependent Protein Kinase Kinase 2 (which is involved in energy

balance and perhaps mobile DNA repair activity), and Cell Division Cycle (CDC)-like kinases (which function in chromatin remodeling and DNA metabolism/repair). The kinases encoded by the AC of Fol4287 include the second copy of a TOR kinase paralog (a top regulator that dictates cellular stress responses) (65); choline kinase (a conserved APH superfamily member involved in antibiotic resistance); a cAMP/G protein-coupled receptor (GPCR); a TOMM system kinase/cyclase fusion protein; and the serine/threonine kinase protein kinase B (involved in stress responses and signal transduction).

3) *Other shared GO terms.* In addition to phosphorylation, the other shared GO term involved in the post-translational modification of proteins is protein ADP-ribosylation (GO:0006471) ($p = 2.99 \times 10^{-8}$ for MRL8996 AC genes and $p = 5 \times 10^{-3}$ for Fol4287 AC genes). These proteins contain a poly(ADP)-ribose polymerase (PARP) catalytic domain (IPR012317) with different combinations of a WGR domain (IPR008893) and a BRCT domain (IPR001357), which regulate protein–DNA or protein–protein interactions, respectively. Several transporter genes, including a chromate transporter gene (GO:0015703), genes enriched in the terms potassium ion transport and iron ion transport, and a hydroxymethylglutaryl-CoA reductase gene (GO:0015936), the rate-limiting enzyme for ergosterol biosynthesis, were also enriched in both genomes (see **Fig. 5C**, **Table S5** and **Table S6** for details).

Fol4287 AC genes are uniquely enriched for defense responses and signaling

Among the best characterized Fol4287 AC genes are *SIX* effector genes, encoding *bona fide* fungal virulent factors (66–68) that are directly involved in fungal–plant interactions. Many genes identified in this study were reported previously. In addition, this study revealed a significant enrichment of Fol4287 AC genes in the GO term defense response (GO:0006952)

compared to the core genes and the AC genes from MRL8896 **(Figure 6 category I and Table S6)**. The AC genes in this group include two chitinase II genes and one patatin-like phospholipase gene involved in the manipulation of plant resistance proteins (69).

Other uniquely enriched GO terms in Fol4287 include phospholipid catabolism (GO:0009395), peptidyl-citrulline biosynthesis-related genes (GO:0018101), and regulation of apoptosis (GO:0042981). The Fol4287 AC genes include 10 encoding phospholipase B enzymes under the GO term phospholipid catabolism that are predicted to have lysophospholipase and transacylase activities and are involved in cellular signaling. Similarly, seven protein-arginine deaminase genes under the GO term peptidyl-citrulline biosynthesis encode proteins that citrullinate numerous proteins, including histones. Several cytochrome P450s, including those in the enriched GO term regulation of apoptosis, were predicted to function in the regulation of apoptosis via their BCL2-like domains (IPR002475). Notably, both citrulline and this group of cytochrome P450s are involved in the biosynthesis of nitric oxide, a key signaling molecule involved in fungal–plant interactions (70, 71).

In addition, functions related to fungal cell wall dynamics, including peptidoglycan biosynthesis (GO:0009252) and peptidoglycan catabolism (GO:0009253), were uniquely enriched among Fol4287 AC genes, as were genes potentially involved in secondary metabolite biosynthesis, including hopanoid biosynthesis (GO:0019746), and genes encoding terpenoid cyclases and clavaminic acid synthetase (IPR003819). One interesting observation is the unique expansion of L-lactate/malate dehydrogenase genes, with 19 paralogs, which function in the tricarboxylic acid cycle (GO:0006096, GO:0006100, and GO:0044262).

MRL8996 AC genes are uniquely enriched for metal ion transport and catabolism

Whereas MRL8996 ACs lack *SIX* effector genes and genes encoding plant cell wall–degrading enzymes, unlike plant pathogenic *F. oxysporum* strains (32), they are uniquely enriched in genes involved in the transport and catabolism of metal ions such as copper, zinc, magnesium (GO:0006825 and GO:0030001), and mercury (GO:0046413) **(Figure 6 category II and Table S5)**. Nine genes are specifically involved in copper ion transport, with seven Ctr-type copper transporter paralogs and two copper-exporting P-type ATPase (CopA) paralogs encoding proteins that also contain multiple copies of the copper chaperone (CopZ) domain. Other genes included in these categories encode a CorA-like magnesium/zinc transporter, with multiple copies of ankyrin repeats, and a Zrt-like, Irt1-like protein (ZIP)-type zinc ion transporter. Most of these genes are present in the genome of another clinical isolate, NRRL32931 (25 out of 33 genes). One of these shared genes encodes a mammalian ceruloplasmin homolog with two multicopper oxidase domains. Homologous sequences were previously detected among a few other opportunistic fungal pathogens and bacteria isolated from extreme environments, but not in any plant pathogenic *Fusarium* species (32), suggesting that a host-specific gene network evolved in the human pathogens.

Another GO term that was exclusively enriched in the MRL8996 ACs is regulation of ligase activity (GO:0051340). This GO term includes two paralogs encoding Tubulin-tyrosine ligase, which harbor a YheC/D-like ATP-grasp fold toward their C terminus, suggesting that this protein may be involved in the modification/biosynthesis of the spore wall and capsular proteins.

Taken together, our results provide strong evidence suggesting that different ACs acquired by a plant or a human pathogen perform shared functions that are essential for chromatin modifications, transcriptional regulation, and post-translational modification of proteins. These essential regulatory mechanisms, which are involved in environmental sensing

and cellular signal transduction, may hold keys to understanding the crosstalk between the core and AC genomic regions. The strain-specific AC gene repertoires may offer hints about the unique adaptations important for fungal survival in different environments and hosts.

DISCUSSION

The FOSC, a group of cross-kingdom fungal pathogens, includes both plant and animal pathogens. Our *in vivo* assays using animal and plant hosts confirmed the host specificity of the keratitis strain MRL8996 and the tomato pathogen Fol4287, as corneal infection with the keratitis strain resulted in significantly more corneal ulceration, while the plant pathogen caused significantly more wilt symptoms among all inoculated tomato seedlings. Consistent with host-specific adaptations, the keratitis strain MRL8996 grew significantly better at elevated temperature, whereas the tomato pathogen Fol4287 exhibited more tolerance to other stress conditions, such as osmotic and cell wall stress. As the first line of fungal adaptation, a human pathogen must overcome the host defenses associated with mammalian endothermy and homeothermy, while a plant pathogen must handle different stresses, such as a rapid oxidative burst (72, 73). Our findings reveal interconnected fungal responses toward biotic stress from plant and animal hosts and abiotic stress in distinct environments. The distinct phenotypes observed in our *in vivo* and *in vitro* assays, together with the identification of unique ACs in each genome, lay the foundation for dissecting cross-kingdom fungal pathogenicity using this comparative model.

The widespread occurrence of the caspofungin paradoxical effect underscores the complexity of antifungal drug responses in filamentous fungi and provides an early warning about the potential complexity in treating infectious diseases caused by *Fusarium* species (74). In the current study, we detected the caspofungin paradoxical effect, but only for the keratitis strain MRL8996. Mechanisms underlying this phenomenon likely involve intricate interplay between

drug–target interactions (75), fungal stress responses (76), and cellular signaling pathways (77–80, 74, 81). Future studies of these mechanisms are essential for devising strategies to overcome the paradoxical effect and for improving the efficacy of antifungal therapies.

In addition, we observed severe disease phenotypes from *Fusarium* keratitis compared to other fungal infections. For instance, corneal infection by *A. fumigatus* requires 40,000 conidia as the inoculum (82). When we used the same titer of *F. oxysporum* conidia, almost all animals developed corneal ulceration and perforation within 24 h. Therefore, we lowered the inoculum to 5,000 conidia. Nevertheless, we still observed over 75% corneal ulceration among eyes inoculated with the human pathogen. This hypervirulence may contribute to the observation that *Fusarium* is the leading cause of blindness among fungal keratitis patients (3, 5).

A unique advantage of our comparative system is the compartmentalized genomic structures for both pathogens, allowing for two distinct sets of ACs to be discovered and compared. Both ACs are repeat rich, yet they are enriched for different families of transposons: while DNA transposons dominate Fol4287 ACs, retrotransposons, especially LINE transposons, are highly abundant among MRL8996 ACs. Importantly, these ACs carry strain-specific genes that contribute to plant and human virulence, respectively. Intriguingly, ACs from both genomes also encode proteins with shared functions, including protein phosphorylation and transcriptional regulation, as supported by our previous finding (65, 26) that kinase and transcription factor genes have proportionally expanded according to the sizes of AC genes in a genome. In the current study, we discovered the enrichment of AC genes contributing to chromatin assembly/disassembly in both strains. *F. oxysporum* ACs, enriched in repetitive sequences, are primarily composed of facultative heterochromatin (54). Establishing the ability to effectively open or close AC regions, either to exploit transcriptional networks or to allow genome

maintenance activities, likely plays a crucial role in the adaptation of this group of fungal pathogens. Our observation of the shared enrichment for genes involved in chromatin assembly and disassembly points to the importance of chromatin remodeling regardless of host-specific functions. Identifying master regulators of the crosstalk between ACs and core components, especially those regulating the activities of both plant and animal pathogens, should uncover unexplored targets for the control of this cross-kingdom pathogen.

In summary, this is the first study documenting a correlation between the genotypes and phenotypes of two closely related pathogens: one infecting humans and one infecting plants. Our established model system, including *in vivo* and *in vitro* assays, makes dissecting adaptation under unique environmental stress conditions feasible. In addition to host-specific virulence, we also observed cross-kingdom virulence, as the human pathogen also colonized plant roots and the plant pathogenic strain infected corneas, although both resulted in milder disease symptoms. More in-depth research is needed on the molecular mechanisms underlying species divergence and adaptation among this group of pathogens.

MATERIALS AND METHODS

Fungal strains

The genome of *F. oxysporum* Fol4287 was first sequenced in 2010 (21), and an improved genome assembly was subsequently produced in 2018 (53). The strain is deposited in multiple public strain repositories, including the Fungal Genetics Stock Center (FGSC 9935), NCAUR/USDA (NRRL 34936), and CBS-KNAW (CBS 123668). The keratitis strain *F. oxysporum* MRL8996 was originally isolated in 2006 from the cornea of a patient with the contact lens–associated multistate outbreak fungal keratitis at Cleveland Clinic Foundation in

Ohio, USA (34). The strain is available at NCAUR/USDA (NRRL 47514). MRL8996 is grouped with other human pathogenic isolates belonging to clade FOSC 3-a. The genome assembly for MRL8996 was produced using the same sequencing technologies and computational strategies used to assemble the Fol4287 genome to facilitate effective comparative analysis (32).

Fungal growth conditions

The conidia of the fungal strains were stored at −80°C in an ultra-freezer in 25–50% (v/v) glycerol for long-term storage and propagated from stocks in liquid potato dextrose broth (PDB, BD Difco™, USA) or potato sucrose broth (PSB: 25% [w/v] boiled potato and 0.5% [w/v] sucrose) for at least 4 days in a shaking incubator at 28°C. The conidia were collected by filtering the liquid fungal cultures through two layers of Miracloth (EMD Millipore). The filtrate was centrifuged at 3700 g for 5 minutes and the spores were resuspended in sterile water to the desired concentration. The spore titers were determined using a hemocytometer.

Mouse corneal infection

Fungal conidia were harvested from Sabouraud Dextrose Agar (SDA) medium and resuspended in phosphate buffered saline (PBS, pH 7.0). Mice were anesthetized by intraperitoneal injection with ketamine/xylazine. A 30-gauge needle was used to make a pocket in the corneal stroma, after which a 33-gauge Hamilton syringe was inserted, and a 5×10^3 conidial suspension in PBS was injected into the corneal stroma. Corneal opacity was photographed using a high-resolution stereo fluorescence MZFLIII microscope (Leica Micro-systems) and a Spot RT Slider KE camera (Diagnostics Instruments). All images were captured using SpotCam software (RT Slider KE; Diagnostics Instruments). Corneal opacity was quantified using Metamorph software. The murine corneal infection model was clinically scored as outlined by Beisel et al. (41). This system categorizes infection severity on a 0–4 scale, primarily based on ulceration size. A score

of 0 indicates an eye similar to the uninfected control eye, 1 indicates low corneal opacity, 2 indicates more severe corneal opacity, 3 indicates dense opacity across the entire anterior segment, and 4 indicates corneal perforation and ocular phthisis.

Colony-forming units (CFUs) from *Fusarium*-infected corneas

Infected whole eyes were homogenized in 1 mL of sterile PBS using a Retsch Mixer Mill MM300 (Qiagen, Valencia, CA) at 33 Hz for 4 min. Ten-fold dilutions were made, and the samples were plated on SDA plates and incubated at 34°C for 48 h. CFUs were determined by direct counting.

Flow cytometry

Infected corneas were dissected, the vascularized iris was removed, and the corneas were incubated in 500 μL collagenase type I (Sigma-Aldrich) at a titer of 82 U per cornea for 1–2 h at 37°C. The cells were resuspended in 200 μL FACS buffer containing 4 μg/cornea Fc blocking Ab (anti-mouse CD16/32; eBioscience) on ice for 10 min, followed by incubation with anti-mouse antibodies against CD45, Ly6G CD11b, or Ly6C, all from BioLegend. Total cells were examined in an ACEA Novocyte™ flow cytometer and analyzed.

Phenotyping of isolates

Yeast extract peptone dextrose (YPD) plates were used as complete medium, and modified Czapek-Dox plates were used as minimal medium. The pH levels of both media were adjusted to pH 7.4 using 6.5% (w/v) 0.1 M citric acid and 43.5% (w/v) 0.2 M Na_2HPO_4. YPD plates containing 0.6 M NaCl, 1 mM H_2O_2, and 1 mg/mL Congo Red were prepared for osmotic, oxidative, and cell wall stress treatments, respectively. Each isolate was grown in PSB for 4 days at 28°C, and the conidia were filtered as described above. Plates containing the same medium were inoculated with 2 μL of spore suspensions at concentrations of 5×10^6, 5×10^5, or 5×10^4 conidia/mL, each in three replicates. The plates were incubated at 28°C or 34°C for 3 days and photographed once a day.

Statistical analysis of growth rates

The growth rates of each replicate and dilution were calculated as the slope of the 3-day growth curve. Five-way ANOVA with a linear model was performed for the following groups: strain, temperature, medium, dilution, and replicate, followed by a multi-comparison with strains, temperatures, and media groups to identify significant differences using MATLAB. To quantify adaptation to different temperatures, the growth rates of cultures with an initial inoculum of 1×10^3 conidia were measured in triplicate. The values of the three replicates incubated at 34°C were normalized to the values of the three replicates incubated at 28°C (total of nine values). A two-way Student's *t*-test was performed between Fol4287 and MRL8996 values. Similarly, to quantify the effects of stress treatment, the values of the three replicates of samples in medium containing different stress components were normalized to the values of the three replicates in control YPD medium (total of nine values), followed by a two-way Student's *t*-test between Fol4287 and MRL8996 in MATLAB.

Caspofungin sensitivity assay

Both strains were maintained in potato dextrose agar (PDA) medium. For solid medium, 2% (w/v) agar was added. The growth rate was determined by spotting 1×10^4 conidia in the center of a 90-mm Petri plate containing 20 mL of solid PDA medium and incubating the plates at 28°C. The diameter was scored at 24-h intervals until 5 days (96 h) of incubation with three biological replicates. To assess the germination kinetics of the strains, 1×10^4 conidia of each strain were inoculated onto glass coverslips containing 200 µL liquid PDA medium, and the samples were incubated for 24 h at 28°C. A conidiospore was counted as germinated if it possessed a germ tube, which was readily detectable as a small protuberance on the spherical spore surface. Two hundred conidia were counted in each experiment.

Plant infection assay

Seeds of tomato (*Solanum lycopersicum*) cv. M82 were maintained in the dark at 4°C for 3 days. The seeds were surface sterilized in 70% (v/v) ethanol for 5 min and washed with 2.7% (w/v) sodium hypochlorite (NaClO) for 5 min. After removing the NaClO solution, the seeds were rinsed with sterile distilled water (SDW) three times. The seeds were then sown in pots filled with autoclaved soil (Promix BX) and watered with SDW. The soil was gently removed from the roots of 10-day-old tomato seedlings by rinsing them with abundant distilled water and SDW while avoiding root tissue damage. The roots of seedlings were inoculated by dipping into the respective human or plant pathogenic *Fusarium* spore suspension (10^6 spores/mL) or in SDW as a mock infection control, for 45 min, before replanting the infected seedlings in soil. After infection, all seedlings were maintained in a growth chamber at 28°C under a 14-h-light/10-h-dark photoperiod.

The fungal strains were maintained in 50% (v/v) glycerol at −80°C, recovered in PDA medium, and transferred to liquid NO_3-based medium (1.7 mg/mL yeast nitrogen base, 30 mg/mL sucrose, and 10.1 mg/mL KNO_3) to promote sporulation. Following staining as previously described (Ghareeb et al. 2011), the infected roots were observed under an Olympus FluoView FV1000 confocal microscope (Tokyo, JP) and photographed with a Hamamatsu camera (Hamamatsu, JP).

Contour-clamped homogeneous electric field (CHEF) electrophoresis

Harvested conidia sample was washed with sterile water, followed by 1.2 M KCl, resuspended in protoplasting solution (25 mg/mL driselase, 5 mg/mL lysing enzyme from Sigma-Aldrich, and 1.2 M KCl), and incubated overnight at 30°C under shaking at 80 rpm. The protoplasts were centrifuged at 4°C for 15 min at 1,000 g, washed by slowly resuspending in 10 mL STC buffer (1 M sorbitol, 10 mM Tris-HCl pH 7.4, and 10 mM $CaCl_2$), and centrifuged again as above. The supernatant was carefully poured out, and the protoplasts were resuspended in STE buffer (2% [w/v] SDS, 0.5 M Tris-HCl pH 8.1, and 10 mM EDTA) to a titer of 2×10^8 conidia/mL. The protoplasts were incubated at 50°C for 10 min and mixed at a 1:1 (v/v) ratio with 1.2% (w/v) Bio-Rad Certified Low Melt Agarose. The mixture was transferred to CHEF Disposable Plug Molds and stored at 4°C for long-term storage. CHEF gel electrophoresis was performed as previously described (83). Briefly, the CHEF Mapper System (Bio-Rad) with 1% (w/v) SeaKem® Gold Agarose (Lonza) in 0.5× Tris borate EDTA (TBE) buffer was used to separate chromosomes at 4–7°C for 260 h. The switching time was 1,200 to 4,800 s at 1.5 V/cm, and the angle was 120°. The running buffer was changed every 2–3 days. The gels were stained with 3× GelGreen (Biotium).

Genome alignment

The alignments of the Fol4287 and MRL8996 nuclear and mitochondrial genomes with repeats masked were generated using MUMmer version 3.23 (84) with the option 'nucmer --maxmatch'. Alignments less than 1 kb were removed using 'delta-filter -g -l 1000'. The extent of sequence identity was calculated for each chromosome by multiplying the percentage sequence identity for each alignment by the length of the alignment averaged over the total length of alignments for the chromosome. The circular plot was generated using Circos (85). Only alignments longer than 5 kb and contigs longer than 5 kb were considered. Contigs from the same chromosome were concatenated. A sequence alignment plot for the mitochondrial genome was generated via a PlotMUMmerAlignments.m script (available at https://github.com/d-ayhan/tools). The annotation of the Fol4287 genome was obtained from the 2010 assembly, while the MRL8996 genome was annotated *de novo* at JGI (86, 87). The genes in ACs were identified and their enriched Gene Ontology (GO) terms analyzed. For Fol4287 genes, locus tag IDs starting with 'FOXG_' were used, while for MRL8996, the 'protein_id' numbers assigned by JGI were used.

Repeat analysis

Repeats were *de novo* identified and classified using RepeatModeler v1.0.11 (88). A previously curated library of 69 transposable elements (TEs) was included in the repeat sequence database. Usearch with the option '-id 0.75' was used to cluster the sequences around centroid repeat sequences, and the annotations were fixed manually (89). RepeatMasker version 4.0.7 was used to mask and annotate the genome assemblies (90). TECNEstimator, a bioinformatics pipeline used to quantify the copy numbers of repeat sequences using short reads from whole-genome sequencing data (SRA accessions: SRP140697 and SRP214968), was used to estimate read counts (available at https://github.com/d-ayhan/TECNEstimator). The counts were normalized to

the median read coverages of the samples. For both genomes, only one representative sequence in a cluster with the highest copy number was selected for downstream analysis.

GO term enrichment analysis

The genes harbored by ACs were identified as those located in AC contigs of MRL8996 and AC and unmapped contigs of Fol4287. The orthologous genes were identified using OrthoFinder version 2.3.3 with default options (91). GO terms for the Fol4287 and MRL8996 genomes were downloaded from JGI Mycocosm (JGI-specific genome identifiers: Fusox2 and FoxMRL8996, respectively) (86). The GO_term_enrichment_analysis.m script (available at https://github.com/d-ayhan/tools), which utilizes the hypergeometric cumulative distribution function, was used to analyze the enriched GO terms in ACs. The proteins encoded by the genes included in each term were subjected to conserved domain analysis using an InterPro-based annotated file provided by JGI and a NCBI conserved domain database CD-Search (https://www.ncbi.nlm.nih.gov/Structure/cdd/wrpsb.cgi).

Phylogenetic analysis

The protein sequence alignments were generated by MEGA11 (92) using the ClustalW algorithm. The phylogenetic tree was reconstructed using FastTree (93) with default options and visualized in iTOL (94).

Acknowledgements

The authors thank the University of Massachusetts High Performance Computing Center for providing the high-performance computing capacities and assisting in data analysis; we also

thank Chris Joyner and David O'Neil of the College of Natural Sciences Greenhouse at the University of Massachusetts, Amherst, for continued support with plant propagation. This project was supported by the National Eye Institute of the National Institutes of Health (R01EY030150) and the Natural Science Foundation (IOS-165241). L.-J.M. is also supported by an Investigator Award in Infectious Diseases and Pathogenesis by the Burroughs Wellcome Fund BWF-1014893; SM is also supported by a Vaadia-BARD Postdoctoral Fellowship. The work (proposal: 10.46936/10.25585/60001360) conducted by the U.S. Department of Energy Joint Genome Institute (https://ror.org/04xm1d337), a DOE Office of Science User Facility, is supported by the Office of Science of the U.S. Department of Energy operated under Contract No. DE-AC02-05CH11231. The funding bodies played no role in the design of the study, the collection, analysis, and interpretation of the data, or the writing of the manuscript.

Author contributions

L.-J.M., D.H.A., and E.P. designed this study. D.H.A. and L.-J.M. wrote the manuscript with input from all authors. D.H.A., S.M., and V.S. S. H. performed data analysis. D.H.A., S.A., D.M.S, K.R., S.K., M.E.M, and M.C.R. performed experiments. T.A, I.V.G, N.S, E.P and L.-J.M. provided funding supports for all experiments and analysis.

Figure 1. *In vivo* pathogenicity assay of clinical (MRL8996) and agricultural (Fol4287) *F. oxysporum* strains using the mouse keratitis model.

A. Representative infected mouse corneas (n = 4) at 24 h after injecting swollen conidia directly into the corneal stroma. The red arrows indicate corneal ulcers where the corneal epithelium has been perforated. **B.** Disease severity, as measured by the clinical score (41) and percent infected corneas with ulcers, showing significant differences between MRL8996- and Fol4287-infected corneas (* $p < 0.01$). A score of 0 indicates an appearance like the uninfected control eyes, 1 represents low corneal opacity, 2 indicates more severe corneal opacity, 3 denotes dense opacity across the entire anterior segment, and 4 indicates corneal perforation and ocular phthisis. **C.** Viable conidia from infected corneas at t = 0 (inoculum; inoculated with 5,000 conidia) and after 24 h, as indicated by the number of colony-forming units (CFUs) (*** $p < 0.001$). **D.** Gating strategy used for flow cytometry. Total cells were isolated from collagenase-digested corneas at 24 h post-infection (hpi) with MRL8996 (top panels) or Fol4287 (bottom panels). Cells were separated by incubating (i) total cells with antibodies against CD45 for myeloid cells (ii); CD45+ myeloid cells with antibodies against Ly6G and CD11b for neutrophils; (iii) CD11b+ cells with antibodies against Ly6C for monocytes. **E., F.,** Quantification of neutrophils (**E**) and monocytes (**F.**) in infected corneas at 24 hpi. Significance was determined by a paired Student's *t*-test, where $p < 0.05$ was considered significant.

Figure 2. *In vivo* pathogenicity assay of clinical (MRL8996) and agricultural (Fol4287) *F. oxysporum* strains using the tomato vascular disease model.

A. Representative photographs of tomato plants inoculated with MRL8996, water (mock), or Fol4287. Ten-day-old tomato seedlings were infected and imaged 10 days later. Twelve of the 20 inoculated seedlings are shown. **B.** Distribution of disease indexes for 20 inoculated tomato seedlings. A disease index of 1–5 was used to measure disease severity as described previously (95): 1 for healthy plants; 2 for plants showing wilted leaves with chlorotic areas; 3 for plants with necrotic spots; 4 for plants with wilted leaves and whole plants showing chlorosis, areas of necrosis, and defoliation; and 5 for dead plants. **C**. Tracking the colonization of the plant pathogen Fol4287 using confocal microscopy. At 4 dpi, Fol4287 reached the xylem in both primary and lateral roots. Fungal hyphae (in green) were stained with WGA-Alexa Fluor 488 and detected by excitation at 488 nm and emission at 500 to 540 nm. Plant tissues (in red) were stained with propidium iodide and detected with excitation at 561 nm and emission at 580–660 nm. **D**. The human keratitis strain MRL8996 colonizes the epidermis and part of the cortex in primary and lateral roots but never enters the xylem in primary or lateral roots. The cluster of fungal structures (in green) indicates some active fungal growth inside plant cells. Scale bars, 50 µm.

Figure 3. *In vitro* growth of clinical (MRL8996) and agricultural (Fol4287) *F. oxysporum* strains subjected to abiotic stress.

A. Colony morphology of MRL8996 and Fol4287 on minimal medium (modified Czapek-Dox agar) pH ~5, minimal medium pH 7.4, complete medium (CM, yeast extract peptone dextrose [YPD] agar), pH ~5, complete medium pH 7.4, osmotic stress medium (potato dextrose agar [PDA] containing 0.6 M NaCl), oxidative stress medium (PDA with 1 mM hydrogen peroxide [H_2O_2]), and cell wall stress medium (YPD with 1 mg/mL Congo Red). The plates were incubated at 28°C or 34°C. The images are representative of three replicates and were taken at 2 days post-inoculation **B.** Ratio of the growth rates (GRs) of colonies under the same conditions as in **A**. at 34°C and 28°C ($GR_{34°C}/GR_{28°C}$) as a representation of temperature adaptation. **C.** Ratio of mean rates of growth under stress conditions (GR_{stress}) and in CM (GR_{normal}) as a representation of stress tolerance at 28°C and 34°C. Data points indicate each growth rate value at 34°C normalized to each growth rate value at 28°C, with each bar showing the mean value. * $p < 0.05$, ** $p < 10^{-5}$; *** $p < 10^{-9}$, calculated by a two-sample *t*-test.

Figure 4. *F. oxysporum* keratitis strain MRL8896 exhibits a paradoxical effect to caspofungin.

A. Representative images of radial fungal growth in the presence of caspofungin. **B.** Ratio of growth rates (GRs) for colonies in the presence of caspofungin (treatment) and in the absence of caspofungin (control). **C.** Effect of caspofungin concentration on germination time. For each strain, 1×10^4 conidia were inoculated onto glass coverslips containing 200 µL of liquid PDA medium and incubated at 28°C for 24 h. Two hundred conidia were counted, and the percent germination was calculated at 0, 2, 4, 6, 8, and 12 h. The time when 50% of the spores germinated was calculated based on the closest datapoint in a log-logistic regression.

Figure 5. Compartmentalized genomes of the clinical (MRL8996) and agricultural (Fol4287) *F. oxysporum* strains.

A. Contour-clamped homogeneous electric field (CHEF) gel of small accessory chromosomes (ACs) of the agricultural isolate Fol4287, the control clinical isolate NRRL32931, and the clinical isolate MRL8996. *S. pombe* (left) and *H. wingei* (right) were used as markers. The band sizes are shown in Mb. ACs are typically below 2 Mb in size, except for two known ACs, chr3 and chr6 in Fol4287, which are much larger due to recent segmental duplications (21). **B.** Whole-genome comparison between MRL8996 and Fol4287 revealed 11 homologous core chromosomes (light green and light blue, respectively) and accessory sequences (dark green and dark blue, respectively) (i). The accessory sequences typically displayed low gene density (ii) and high repetitive sequence composition (iii). The syntenic alignment between MRL8996 and Fol4287 using nucmer (iv) indicates the accessory regions lacking synteny between MRL8996 and Fol4287. **C.** Distribution of all identified transposable elements in the Fol4287 (upper panel) and MRL8996 (lower panel) genomes, consisting of class I retrotransposons, class II DNA transposons, and unknown transposable elements. **D.** Transposon abundance in the Fol4287 and MRL8996 genomes. Class I retrotransposons include LTRs (long terminal repeats), LINEs (long interspersed nuclear elements), and SINEs (short interspersed nuclear elements). Class II DNA transposons are classified into TIRs (terminal inverted repeats) and Helitrons.

Figure 6. Enriched Gene Ontology terms among accessory genes of the clinical (MRL8996) and agricultural (Fol4287) *F. oxysporum* isolates.

Enriched Gene Ontology (GO) terms harbored by the ACs from Fol4287 (green) and MRL8996 (blue). Category I represents GO terms enriched in Fol4287 ACs. Category II represents GO terms enriched in the ACs of both genomes. Category III represents GO terms enriched in MRL8996 ACs. For graphical representation, a *p*-value = 0 is shown as −log10(*p*-value) = 30.

Table 1. Comparative annotation of the Fol4287 and MRL8996 genomes.

	Fol4287	**MRL8996**
Total genes	20,925	16,631
Genes with GO annotation	9,783	7,958
Total AC genes	3,890	2,017
AC genes with GO annotation	1,788	542

Figure S1. Unedited photographs of plants infected with Fol4287 or MRL8896 or mock-infected with water (Mock) at 12 dpi.

Figure S2. *In vitro* growth assays of MRL8996 and Fol4287 strains under different abiotic stress conditions.

Figure S3. Dotplot showing the sequence identity between the mitochondrial genomes of Fol4287 and MRL8996.

Figure S4. Counts of unknown repeat families in the Fol4287 (green) and MRL8996 (blue) genomes.

Figure S5. Phylogeny of proteins involved in chromatin assembly and disassembly encoded by genes located on the accessory chromosomes of Fol4287 and MRL8996.

REFERENCES

1. World Health Organization. 2022. WHO fungal priority pathogens list to guide research, development and public health action. https://www.who.int/publications-detail-redirect/9789240060241.

2. Dean R, Van Kan JA, Pretorius ZA, Hammond-Kosack KE, Di Pietro A, Spanu PD, Rudd JJ, Dickman M, Kahmann R, Ellis J, Foster GD. 2012. The Top 10 fungal pathogens in molecular plant pathology. Mol Plant Pathol, 2012/04/05 ed. 13:414–430.

3. Kredics L, Narendran V, Shobana CS, Vágvölgyi C, Manikandan P, Indo- Hungarian Fungal Keratitis Working Group. 2015. Filamentous fungal infections of the cornea: a global overview of epidemiology and drug sensitivity. Mycoses 58:243–260.

4. Abbondante S, Leal SM, Clark HL, Ratitong B, Sun Y, Ma L-J, Pearlman E. 2023. Immunity to pathogenic fungi in the eye. Seminars in Immunology 67:101753.

5. Hassan AS, Al-Hatmi AMS, Shobana CS, van Diepeningen AD, Kredics L, Vágvölgyi C, Homa M, Meis JF, de Hoog GS, Narendran V, Manikandan P, IHFK Working Group. 2016. Antifungal Susceptibility and Phylogeny of Opportunistic Members of the Genus Fusarium Causing Human Keratomycosis in South India. Med Mycol 54:287–294.

6. Lalitha P, Prajna NV, Manoharan G, Srinivasan M, Mascarenhas J, Das M, D'Silva SS, Porco TC, Keenan JD. 2015. Trends in bacterial and fungal keratitis in South India, 2002-2012. Br J Ophthalmol 99:192–194.

7. He D, Hao J, Zhang B, Yang Y, Song W, Zhang Y, Yokoyama K, Wang L. 2011. Pathogenic spectrum of fungal keratitis and specific identification of Fusarium solani. Invest Ophthalmol Vis Sci 52:2804–2808.

8. Wang L, Sun S, Jing Y, Han L, Zhang H, Yue J. 2009. Spectrum of fungal keratitis in central China. Clin Exp Ophthalmol 37:763–771.

9. O'Sullivan J, Gilbert C, Foster A. 1997. The causes of childhood blindness in South Africa. S Afr Med J 87:1691–1695.

10. Ibrahim MM, Vanini R, Ibrahim FM, Fioriti LS, Furlan EMR, Provinzano LMA, De Castro RS, Sousa SJDFE, Rocha EM. 2009. Epidemiologic aspects and clinical outcome of fungal keratitis in southeastern Brazil. Eur J Ophthalmol 19:355–361.

11. O'Donnell K, Sarver BA, Brandt M, Chang DC, Noble-Wang J, Park BJ, Sutton DA, Benjamin L, Lindsley M, Padhye A, Geiser DM, Ward TJ. 2007. Phylogenetic diversity and microsphere array-based genotyping of human pathogenic Fusaria, including isolates from the multistate contact lens-associated U.S. keratitis outbreaks of 2005 and 2006. J Clin Microbiol, 2007/05/18 ed. 45:2235–2248.

12. Gower EW, Keay LJ, Oechsler RA, Iovieno A, Alfonso EC, Jones DB, Colby K, Tuli SS, Patel SR, Lee SM, Irvine J, Stulting RD, Mauger TF, Schein OD. 2010. Trends in fungal keratitis in the United States, 2001 to 2007. Ophthalmology 117:2263–2267.

13. Michielse CB, Rep M. 2009. Pathogen profile update: Fusarium oxysporum. Mol Plant Pathol, 2009/04/30 ed. 10:311–324.

14. Berger S, Chazli YE, Babu AF, Coste AT. 2017. Azole resistance in Aspergillus fumigatus: A consequence of antifungal use in agriculture? Frontiers in Microbiology.

15. Pfaller MA. 2012. Antifungal drug resistance: mechanisms, epidemiology, and consequences for treatment. Am J Med 125:S3-13.

16. Altus, Viljoen, Li-Jun, Ma, Augusta, Molina. 2020. Fusarium Wilt (Panama Disease) and Monoculture in Banana Production: Resurgence of a Century-Old Disease, p. 159–184. *In* Emerging plant diseases and global food security. A. Records & J. Ristaino, APS Press.

17. Scheel CM, Hurst SF, Barreiros G, Akiti T, Nucci M, Balajee SA. 2013. Molecular analyses of Fusarium isolates recovered from a cluster of invasive mold infections in a Brazilian hospital. BMC Infect Dis 13:49.

18. Nucci M, Marr KA, Vehreschild MJGT, De Souza CA, Velasco E, Cappellano P, Carlesse F, Queiroz-Telles F, Sheppard DC, Kindo A, Cesaro S, Hamerschlak N, Solza C, Heinz WJ, Schaller M, Atalla A, Arikan-Akdagli S, Bertz H, Galvão Castro C, Herbrecht R, Hoenigl M, Härter G, Hermansen NEU, Josting A, Pagano L, Salles MJC, Mossad SB, Ogunc D, Pasqualotto AC, Araujo V, Troke PF, Lortholary O, Comely OA, Anaissie E. 2014. Improvement in the outcome of invasive fusariosis in the last decade. Clinical Microbiology and Infection 20:580–585.

19. Prajna NV, Krishnan T, Rajaraman R, Patel S, Srinivasan M, Das M, Ray KJ, O'Brien KS, Oldenburg CE, McLeod SD, Zegans ME, Porco TC, Acharya NR, Lietman TM, Rose-Nussbaumer J, for the Mycotic Ulcer Treatment Trial II Group. 2016. Effect of Oral Voriconazole on Fungal Keratitis in the Mycotic Ulcer Treatment Trial II (MUTT II): A Randomized Clinical Trial. JAMA Ophthalmol 134:1365.

20. Kistler H. 2001. Evolution of host specificity in Fusarium oxysporum, p. 70–82. *In* Nelson, P, Summerell, B (eds.), Fusarium: Paul E. Nelson Memorial Symposium. APS Press.

21. Ma LJ, van der Does HC, Borkovich KA, Coleman JJ, Daboussi MJ, Di Pietro A, Dufresne M, Freitag M, Grabherr M, Henrissat B, Houterman PM, Kang S, Shim WB, Woloshuk C, Xie X, Xu JR, Antoniw J, Baker SE, Bluhm BH, Breakspear A, Brown DW, Butchko RA, Chapman S, Coulson R, Coutinho PM, Danchin EG, Diener A, Gale LR, Gardiner DM, Goff S, Hammond-Kosack KE, Hilburn K, Hua-Van A, Jonkers W, Kazan K, Kodira CD, Koehrsen M, Kumar L, Lee YH, Li L, Manners JM, Miranda-Saavedra D, Mukherjee M, Park G, Park J, Park SY, Proctor RH, Regev A, Ruiz-Roldan MC, Sain D, Sakthikumar S, Sykes S, Schwartz DC, Turgeon BG, Wapinski I, Yoder O, Young S, Zeng Q, Zhou S, Galagan J, Cuomo CA, Kistler HC, Rep M. 2010. Comparative genomics reveals mobile pathogenicity chromosomes in Fusarium. Nature, 2010/03/20 ed. 464:367–373.

22. Ma L-J, Geiser DM, Proctor RH, Rooney AP, O'Donnell K, Trail F, Gardiner DM, Manners JM, Kazan K. 2013. Fusarium Pathogenomics. Annu Rev Microbiol 67:399–416.

23. Van Dam P, Fokkens L, Schmidt SM, Linmans JHJ, Kistler HC, Ma L-J, Rep M. 2016. Effector profiles distinguish *formae speciales* of *Fusarium oxysporum*: Effector profiles distinguish *Formae speciales* of Fo. Environ Microbiol 18:4087–4102.

24. Yu H, Ayhan DH, Martínez-Soto D, Cochavi SM, Ma L-J. 2023. Accessory Chromosomes of the Fusarium oxysporum Species Complex and Their Contribution to Host Niche Adaptation, p. 371–388. *In* Scott, B, Mesarich, C (eds.), Plant Relationships. Springer International Publishing, Cham.

25. Rep M. 2005. Small proteins of plant-pathogenic fungi secreted during host colonization. FEMS Microbiology Letters 253:19–27.

26. Yu H, Yang H, Haridas S, Hayes RD, Lynch H, Andersen S, Newman M, Li G, Martínez-Soto D, Milo-Cochavi S, Hazal Ayhan D, Zhang Y, Grigoriev IV, Ma L-J. 2023. Conservation and Expansion of Transcriptional Factor Repertoire in the Fusarium oxysporum Species Complex. JoF 9:359.

27. Turrà D, Segorbe D, Di Pietro A. 2014. Protein Kinases in Plant-Pathogenic Fungi: Conserved Regulators of Infection. Annu Rev Phytopathol 52:267–288.

28. López-Berges MS, Rispail N, Prados-Rosales RC, Di Pietro A. 2010. A Nitrogen Response Pathway Regulates Virulence Functions in *Fusarium oxysporum* via the Protein Kinase TOR and the bZIP Protein MeaB. The Plant Cell 22:2459–2475.

29. Kistler HC, Rep M, Ma L-J. 2013. Structural dynamics of Fusarium genomes In: Fusarium: genomics, molecular and cellular biology. Eds. Brown, D.W. and Proctor, R.H., Horizon Scientific Press, Norwich, United Kingdom.

30. Van Dam P, Fokkens L, Ayukawa Y, Van Der Gragt M, Ter Horst A, Brankovics B, Houterman PM, Arie T, Rep M. 2017. A mobile pathogenicity chromosome in Fusarium oxysporum for infection of multiple cucurbit species. Scientific Reports 7.

31. Schäfer K, Di Pietro A, Gow NAR, MacCallum D. 2014. Murine Model for Fusarium oxysporum Invasive Fusariosis Reveals Organ-Specific Structures for Dissemination and Long-Term Persistence. PLoS ONE 9:e89920.

32. Zhang Y, Yang H, Turra D, Zhou S, Ayhan DH, DeIulio GA, Guo L, Broz K, Wiederhold N, Coleman JJ, Donnell KO, Youngster I, McAdam AJ, Savinov S, Shea T, Young S, Zeng Q, Rep M, Pearlman E, Schwartz DC, Di Pietro A, Kistler HC, Ma L-J. 2020. The genome of opportunistic fungal pathogen Fusarium oxysporum carries a unique set of lineage-specific chromosomes. 1. Commun Biol 3:1–12.

33. Schmidt SM, Houterman PM, Schreiver I, Ma L, Amyotte S, Chellappan B, Boeren S, Takken FLW, Rep M. 2013. MITEs in the promoters of effector genes allow prediction of novel virulence genes in Fusarium oxysporum. BMC Genomics 14:119.

34. Chang DC, Grant GB, O'Donnell K, Wannemuehler KA, Noble-Wang J, Rao CY, Jacobson LM, Crowell CS, Sneed RS, Lewis FMT, Schaffzin JK, Kainer MA, Genese CA, Alfonso EC, Jones DB, Srinivasan A, Fridkin SK, Park BJ, Fusarium Keratitis Investigation Team. 2006. Multistate outbreak of Fusarium keratitis associated with use of a contact lens solution. JAMA 296:953–963.

35. O'Donnell K, Sutton DA, Rinaldi MG, Magnon KC, Cox PA, Revankar SG, Sanche S, Geiser DM, Juba JH, Van Burik J-AH, Padhye A, Anaissie EJ, Francesconi A, Walsh TJ, Robinson JS. 2004. Genetic Diversity of Human Pathogenic Members of the *Fusarium oxysporum* Complex Inferred from Multilocus DNA Sequence Data and Amplified Fragment Length Polymorphism Analyses: Evidence for the Recent Dispersion of a Geographically Widespread Clonal Lineage and Nosocomial Origin. J Clin Microbiol 42:5109–5120.

36. O'Donnell K, Sarver BAJ, Brandt M, Chang DC, Noble-Wang J, Park BJ, Sutton DA, Benjamin L, Lindsley M, Padhye A, Geiser DM, Ward TJ. 2007. Phylogenetic Diversity and Microsphere Array-Based Genotyping of Human Pathogenic Fusaria, Including Isolates from the Multistate Contact Lens-Associated U.S. Keratitis Outbreaks of 2005 and 2006. J Clin Microbiol 45:2235–2248.

37. Di Pietro A, Roncero MI. 1996. Purification and characterization of an exo-polygalacturonase from the tomato vascular wilt pathogen Fusarium oxysporum f.sp. lycopersici. FEMS Microbiol Lett 145:295–299.

38. O'Donnell K, Sutton DA, Rinaldi MG, Magnon KC, Cox PA, Revankar SG, Sanche S, Geiser DM, Juba JH, van Burik J-AH, Padhye A, Anaissie EJ, Francesconi A, Walsh TJ, Robinson JS. 2004. Genetic Diversity of Human Pathogenic Members of the Fusarium oxysporum Complex Inferred from Multilocus DNA Sequence Data and Amplified Fragment Length Polymorphism Analyses: Evidence for the Recent Dispersion of a Geographically Widespread Clonal Lineage and Nosocomial Origin. J Clin Microbiol 42:5109–5120.

39. Gordon TR. 2017. *Fusarium oxysporum* and the *Fusarium* Wilt Syndrome. Annu Rev Phytopathol 55:23–39.

40. Edel-Hermann V, Lecomte C. 2019. Current Status of *Fusarium oxysporum Formae Speciales* and Races. Phytopathology® 109:512–530.

41. Beisel KW, Hazlett LD, Berk RS. 1983. Dominant Susceptibility Effect on the Murine Corneal Response to Pseudomonas aeruginosa. Experimental Biology and Medicine 172:488–491.

42. Christensen JE, Andreasen SØ, Christensen JP, Thomsen AR. 2001. CD11b expression as a marker to distinguish between recently activated effector CD8+ T cells and memory cells. International Immunology 13:593–600.

43. Di Pietro A, Roncero MI. 1998. Cloning, expression, and role in pathogenicity of pg1 encoding the major extracellular endopolygalacturonase of the vascular wilt pathogen Fusarium oxysporum. Mol Plant Microbe Interact, 1998/02/05 ed. 11:91–98.

44. Guo L, Yu H, Wang B, Vescio K, DeIulio GA, Yang H, Berg A, Zhang L, Edel-Hermann V, Steinberg C, Kistler HC, Ma L-J. 2021. Metatranscriptomic comparison of endophytic and pathogenic *Fusarium* –Arabidopsis interactions reveals plant transcriptional plasticity. preprint. Plant Biology.

45. Martínez-Soto D, Yu H, Allen KS, Ma L-J. 2023. Differential Colonization of the Plant Vasculature Between Endophytic Versus Pathogenic *Fusarium oxysporum* Strains. MPMI MPMI-08-22-0166-SC.

46. García-Maceira FI, Di Pietro A, Roncero MIG. 2000. Cloning and Disruption of *pgx4* Encoding an In Planta Expressed Exopolygalacturonase from *Fusarium oxysporum*. MPMI 13:359–365.

47. Ghareeb H, Becker A, Iven T, Feussner I, Schirawski J. 2011. Sporisorium reilianum Infection Changes Inflorescence and Branching Architectures of Maize. Plant Physiology 156:2037–2052.

48. Kessel L, Johnson L, Arvidsson H, Larsen M. 2010. The Relationship between Body and Ambient Temperature and Corneal Temperature. Investigative Opthalmology & Visual Science 51:6593.

49. Pfaller MA, Diekema DJ, Messer SA, Hollis RJ, Jones RN. 2003. In Vitro Activities of Caspofungin Compared with Those of Fluconazole and Itraconazole against 3,959 Clinical Isolates of *Candida* spp., Including 157 Fluconazole-Resistant Isolates. Antimicrob Agents Chemother 47:1068–1071.

50. Bowman JC, Hicks PS, Kurtz MB, Rosen H, Schmatz DM, Liberator PA, Douglas CM. 2002. The Antifungal Echinocandin Caspofungin Acetate Kills Growing Cells of *Aspergillus fumigatus* In Vitro. Antimicrob Agents Chemother 46:3001–3012.

51. Ha Y, Covert SF, Momany M. 2006. FsFKS1, the 1,3-β-Glucan Synthase from the Caspofungin-Resistant Fungus *Fusarium solani*. Eukaryot Cell 5:1036–1042.

52. Pfaller MA, Marco F, Messer SA, Jones RN. 1998. In Vitro Activity of Two Echinocandin Derivatives, LY303366 and MK-0991 (L-743,792), Against Clinical Isolates of Aspergillus, Fusarium, Rhizopus, and Other Filamentous Fungi. Diagnostic Microbiology and Infectious Disease 30:251–255.

53. Ayhan DH, López-Díaz C, Di Pietro A, Ma L-J. 2018. Improved Assembly of Reference Genome Fusarium oxysporum f. sp. lycopersici Strain Fol4287. Microbiology Resource Announcements https://doi.org/10.1128/mra.00910-18.

54. Fokkens L, Shahi S, Connolly LR, Stam R, Schmidt SM, Smith KM, Freitag M, Rep M. 2018. The multi-speed genome of *Fusarium oxysporum* reveals association of histone modifications with sequence divergence and footprints of past horizontal chromosome transfer events. preprint. Genomics.

55. Brankovics B, Van Dam P, Rep M, De Hoog GS, J. Van Der Lee TA, Waalwijk C, Van Diepeningen AD. 2017. Mitochondrial genomes reveal recombination in the presumed asexual Fusarium oxysporum species complex. BMC Genomics 18:735.

56. Yang H, Yu H, Ma L-J. 2020. Accessory Chromosomes in *Fusarium oxysporum*. Phytopathology® 110:1488–1496.

57. Chellapan BV, Van Dam P, Rep M, Cornelissen BJC, Fokkens L. 2016. Non-canonical Helitrons in Fusarium oxysporum. Mobile DNA 7:27.

58. Grigoriev IV, Nikitin R, Haridas S, Kuo A, Ohm R, Otillar R, Riley R, Salamov A, Zhao X, Korzeniewski F, Smirnova T, Nordberg H, Dubchak I, Shabalov I. 2014. MycoCosm portal: gearing up for 1000 fungal genomes. Nucl Acids Res 42:D699–D704.

59. Lachner M, O'Carroll D, Rea S, Mechtler K, Jenuwein T. 2001. Methylation of histone H3 lysine 9 creates a binding site for HP1 proteins. Nature 410:116–120.

60. Nakayama J, Rice JC, Strahl BD, Allis CD, Grewal SIS. 2001. Role of Histone H3 Lysine 9 Methylation in Epigenetic Control of Heterochromatin Assembly. Science 292:110–113.

61. Mondal T, Rasmussen M, Pandey GK, Isaksson A, Kanduri C. 2010. Characterization of the RNA content of chromatin. Genome Res 20:899–907.

62. Varadi M, Anyango S, Deshpande M, Nair S, Natassia C, Yordanova G, Yuan D, Stroe O, Wood G, Laydon A, Žídek A, Green T, Tunyasuvunakool K, Petersen S, Jumper J, Clancy E, Green R, Vora A, Lutfi M, Figurnov M, Cowie A, Hobbs N, Kohli P, Kleywegt G, Birney E, Hassabis D, Velankar S.

2022. AlphaFold Protein Structure Database: massively expanding the structural coverage of protein-sequence space with high-accuracy models. Nucleic Acids Research 50:D439–D444.

63. Leopold K, Stirpe A, Schalch T. 2019. Transcriptional gene silencing requires dedicated interaction between HP1 protein Chp2 and chromatin remodeler Mit1. Genes Dev 33:565–577.

64. Schoelz JM, Riddle NC. 2022. Functions of HP1 proteins in transcriptional regulation. Epigenetics & Chromatin 15:14.

65. DeIulio G, Guo L, Zhang Y, Goldberg J, Kistler H, Ma L-J. 2018. Kinome expansion in the Fusarium oxysporum species complex driven by accessary chromosomes. mSphere mSphere 3:e00231-18.

66. van der Does HC, Duyvesteijn RG, Goltstein PM, van Schie CC, Manders EM, Cornelissen BJ, Rep M. 2008. Expression of effector gene SIX1 of Fusarium oxysporum requires living plant cells. Fungal Genet Biol, 2008/07/09 ed. 45:1257–1264.

67. Lievens B, Houterman PM, Rep M. 2009. Effector gene screening allows unambiguous identification of Fusarium oxysporum f. sp. lycopersici races and discrimination from other formae speciales. FEMS Microbiol Lett, 2009/10/06 ed. 300:201–215.

68. van Dam P, Fokkens L, Schmidt SM, Linmans JH, Kistler HC, Ma LJ, Rep M. 2016. Effector profiles distinguish formae speciales of Fusarium oxysporum. Environ Microbiol https://doi.org/10.1111/1462-2920.13445.

69. Houterman PM, Ma L, van Ooijen G, de Vroomen MJ, Cornelissen BJ, Takken FL, Rep M. 2009. The effector protein Avr2 of the xylem colonizing fungus Fusarium oxysporum activates the tomato resistance protein I-2 intracellularly. Plant J, 2009/02/21 ed. 58:970–978.

70. Cánovas D, Marcos JF, Marcos AT, Strauss J. 2016. Nitric oxide in fungi: is there NO light at the end of the tunnel? Curr Genet 62:513–518.

71. Ding Y, Gardiner DM, Xiao D, Kazan K. 2020. Regulators of nitric oxide signaling triggered by host perception in a plant pathogen. Proc Natl Acad Sci USA 117:11147–11157.

72. Lamb C, Dixon RA. 1997. THE OXIDATIVE BURST IN PLANT DISEASE RESISTANCE. Annu Rev Plant Physiol Plant Mol Biol 48:251–275.

73. Segal LM, Wilson RA. 2018. Reactive oxygen species metabolism and plant-fungal interactions. Fungal Genet Biol 110:1–9.

74. Valero C, Colabardini AC, De Castro PA, Amich J, Bromley MJ, Goldman GH. 2022. The Caspofungin Paradoxical Effect is a Tolerant “Eagle Effect” in the Filamentous Fungal Pathogen *Aspergillus fumigatus*. mBio 13:e00447-22.

75. Sumiyoshi M, Miyazaki T, Makau JN, Mizuta S, Tanaka Y, Ishikawa T, Makimura K, Hirayama T, Takazono T, Saijo T, Yamaguchi H, Shimamura S, Yamamoto K, Imamura Y, Sakamoto N, Obase Y, Izumikawa K, Yanagihara K, Kohno S, Mukae H. 2020. Novel and potent antimicrobial effects of caspofungin on drug-resistant Candida and bacteria. Sci Rep 10:17745.

76. Day AM, Quinn J. 2019. Stress-Activated Protein Kinases in Human Fungal Pathogens. Front Cell Infect Microbiol 9:261.

77. García R, Bravo E, Diez-Muñiz S, Nombela C, Rodríguez-Peña JM, Arroyo J. 2017. A novel connection between the Cell Wall Integrity and the PKA pathways regulates cell wall stress response in yeast. Sci Rep 7:5703.

78. Iyer KR, Robbins N, Cowen LE. 2022. The role of Candida albicans stress response pathways in antifungal tolerance and resistance. iScience 25:103953.

79. Pianalto KM, Billmyre RB, Telzrow CL, Alspaugh JA. 2019. Roles for Stress Response and Cell Wall Biosynthesis Pathways in Caspofungin Tolerance in *Cryptococcus neoformans*. Genetics 213:213–227.

80. Ries LNA, Rocha MC, De Castro PA, Silva-Rocha R, Silva RN, Freitas FZ, De Assis LJ, Bertolini MC, Malavazi I, Goldman GH. 2017. The Aspergillus fumigatus CrzA Transcription Factor Activates Chitin Synthase Gene Expression during the Caspofungin Paradoxical Effect. mBio 8:e00705-17.

81. De Castro PA, Colabardini AC, Manfiolli AO, Chiaratto J, Silva LP, Mattos EC, Palmisano G, Almeida F, Persinoti GF, Ries LNA, Mellado L, Rocha MC, Bromley M, Silva RN, De Souza GS, Loures FV, Malavazi I, Brown NA, Goldman GH. 2019. Aspergillus fumigatus calcium-responsive transcription factors regulate cell wall architecture promoting stress tolerance, virulence and caspofungin resistance. PLoS Genet 15:e1008551.

82. Leal SM, Roy S, Vareechon C, Carrion S deJesus, Clark H, Lopez-Berges MS, diPietro A, Schrettl M, Beckmann N, Redl B, Haas H, Pearlman E. 2013. Targeting Iron Acquisition Blocks Infection with the Fungal Pathogens Aspergillus fumigatus and Fusarium oxysporum. PLoS Pathog 9:e1003436.

83. Ayukawa Y, Asai S, Gan P, Tsushima A, Ichihashi Y, Shibata A, Komatsu K, Houterman PM, Rep M, Shirasu K, Arie T. 2021. A pair of effectors encoded on a conditionally dispensable chromosome of Fusarium oxysporum suppress host-specific immunity. Commun Biol 4:1–12.

84. Kurtz S, Phillippy A, Delcher AL, Smoot M, Shumway M, Antonescu C, Salzberg SL. 2004. Versatile and open software for comparing large genomes. Genome biology 5:R12.

85. Krzywinski M, Schein J, Birol İ, Connors J, Gascoyne R, Horsman D, Jones SJ, Marra MA. 2009. Circos: An information aesthetic for comparative genomics. Genome Res 19:1639–1645.

86. Grigoriev IV, Nikitin R, Haridas S, Kuo A, Ohm R, Otillar R, Riley R, Salamov A, Zhao X, Korzeniewski F, Smirnova T, Nordberg H, Dubchak I, Shabalov I. 2014. MycoCosm portal: gearing up for 1000 fungal genomes. Nucleic Acids Research 42:D699–D704.

87. Grigoriev IV, Cullen D, Goodwin SB, Hibbett D, Jeffries TW, Kubicek CP, Kuske C, Magnuson JK, Martin F, Spatafora JW, Tsang A, Baker SE. 2011. Fueling the future with fungal genomics. null 2:192–209.

88. Smit A, Hubley R. 2015. RepeatModeler Open-1.0<http://www.repeatmasker.org>.

89. Edgar R. 2010. Usearch. Lawrence Berkeley National Lab. (LBNL), Berkeley, CA (United States).

90. Smit A, Hubley R, Green P. 2015. RepeatMasker Open-4.0<http://www.repeatmasker.org>. http://www.repeatmasker.org.

91. Emms DM, Kelly S. 2019. OrthoFinder: phylogenetic orthology inference for comparative genomics. Genome Biology 20:238.

92. Tamura K, Stecher G, Kumar S. 2021. MEGA11: Molecular Evolutionary Genetics Analysis Version 11. Molecular Biology and Evolution 38:3022–3027.

93. Price MN, Dehal PS, Arkin AP. 2010. FastTree 2 – Approximately Maximum-Likelihood Trees for Large Alignments. PLoS ONE 5:e9490.

94. Letunic I, Bork P. 2021. Interactive Tree Of Life (iTOL) v5: an online tool for phylogenetic tree display and annotation. Nucleic Acids Research 49:W293–W296.

95. García-Maceira FI, Di Pietro A, Roncero MIG. 2000. Cloning and Disruption of *pgx4* Encoding an In Planta Expressed Exopolygalacturonase from *Fusarium oxysporum*. MPMI 13:359–365.

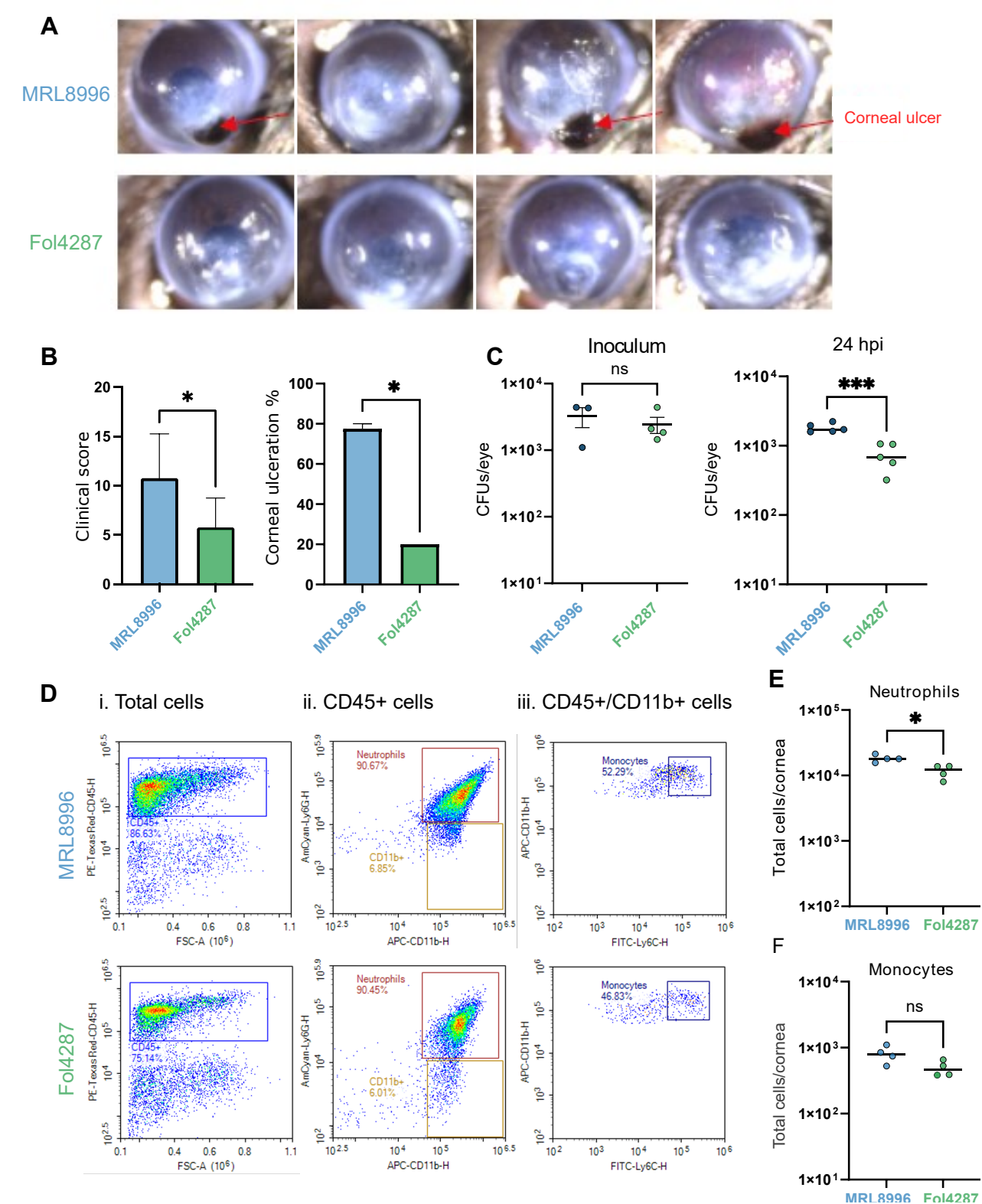
A
MRL8996
Fol4287
Corneal ulcer
B
Clinical score
Corneal ulceration %
MRL8996
Fol4287
C
Inoculum
24 hpi
ns
CFUs/eye
D
i. Total cells
ii. CD45+ cells
iii. CD45+/CD11b+ cells
CD45+ 86.63%
CD45+ 75.14%
Neutrophils 90.67%
Neutrophils 90.45%
CD11b+ 6.85%
CD11b+ 6.01%
Monocytes 52.29%
Monocytes 46.83%
FSC-A (10^6)
APC-CD11b-H
FITC-Ly6C-H
E
Neutrophils
Total cells/cornea
F
Monocytes

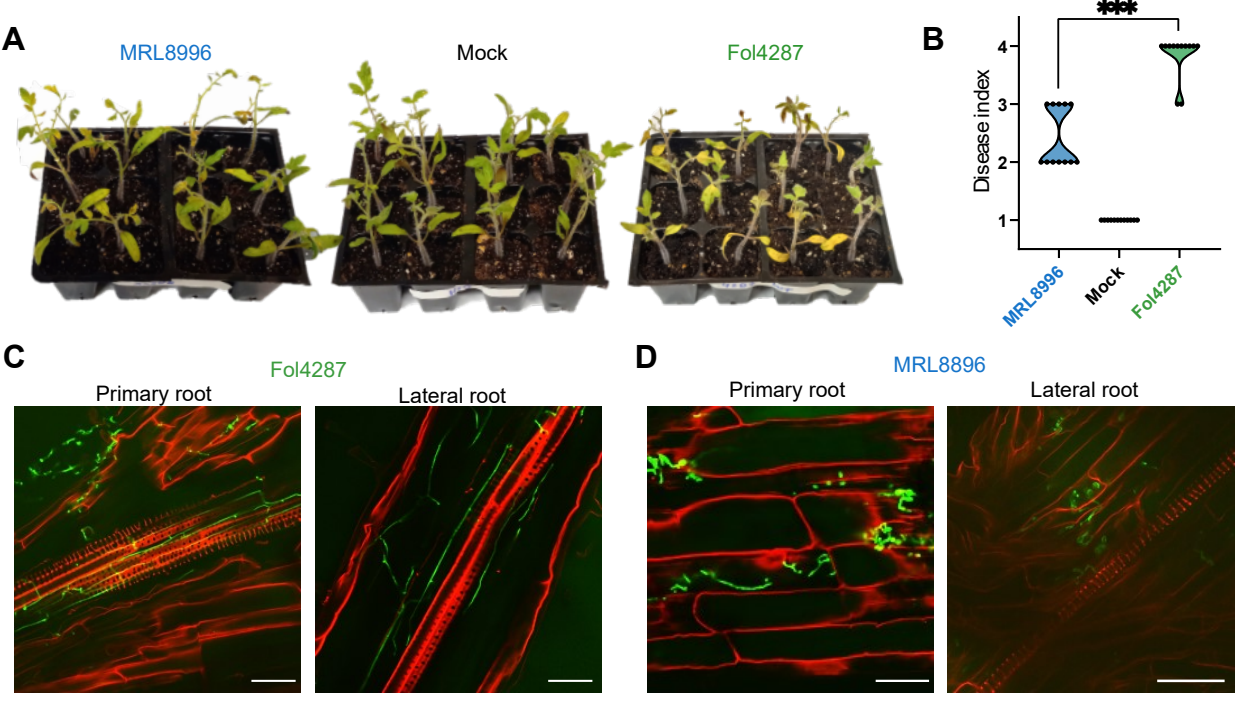
A
MRL8996
Mock
Fol4287
B
***
Disease index
4
3
2
1
MRL8996
Mock
Fol4287
C
Fol4287
Primary root
Lateral root
D
MRL8896
Primary root
Lateral root

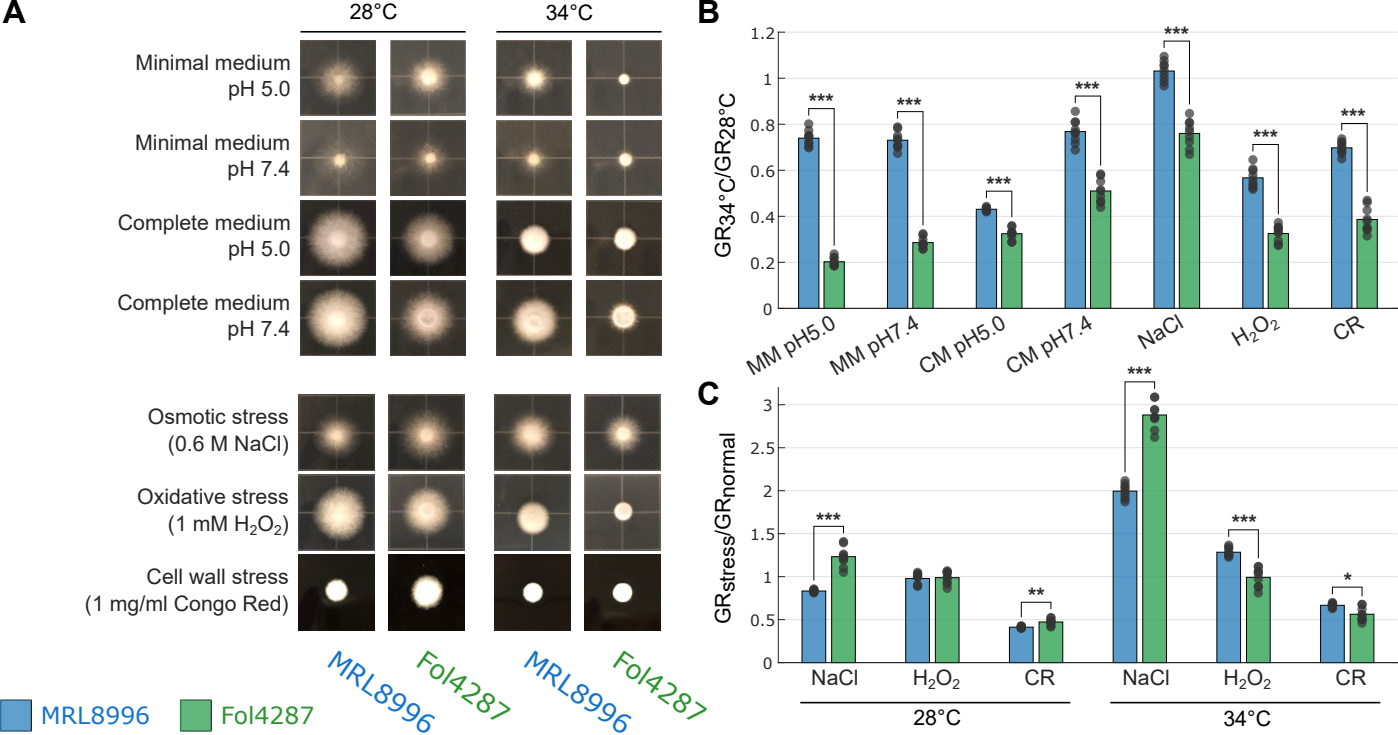
A
28°C
34°C
Minimal medium pH 5.0
Minimal medium pH 7.4
Complete medium pH 5.0
Complete medium pH 7.4
Osmotic stress (0.6 M NaCl)
Oxidative stress (1 mM H_2O_2)
Cell wall stress (1 mg/ml Congo Red)
MRL8996
Fol4287
MRL8996
Fol4287
B
$GR_{34°C}/GR_{28°C}$
MM pH5.0
MM pH7.4
CM pH5.0
CM pH7.4
NaCl
H_2O_2
CR
C
GR_{stress}/GR_{normal}
NaCl
H_2O_2
CR
NaCl
H_2O_2
CR
28°C
34°C
MRL8996
Fol4287

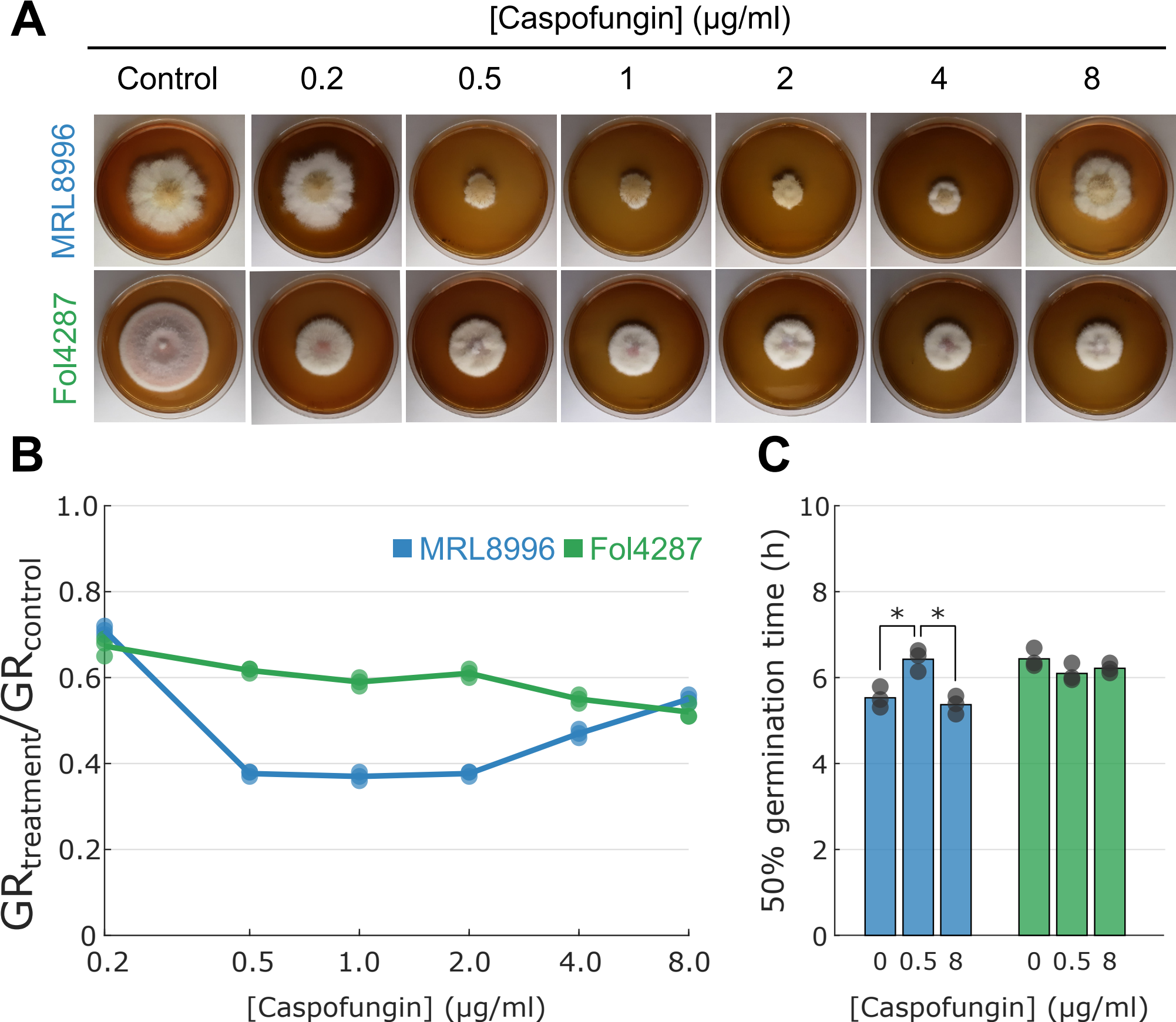
A
[Caspofungin] (µg/ml)
Control
0.2
0.5
1
2
4
8
MRL8996
Fol4287
B
MRL8996
Fol4287
GRtreatment/GRcontrol
1.0
0.8
0.6
0.4
0.2
0
0.2
0.5
1.0
2.0
4.0
8.0
[Caspofungin] (µg/ml)
C
50% germination time (h)
10
8
6
4
2
0
*
*
0
0.5
8
0
0.5
8
[Caspofungin] (µg/ml)

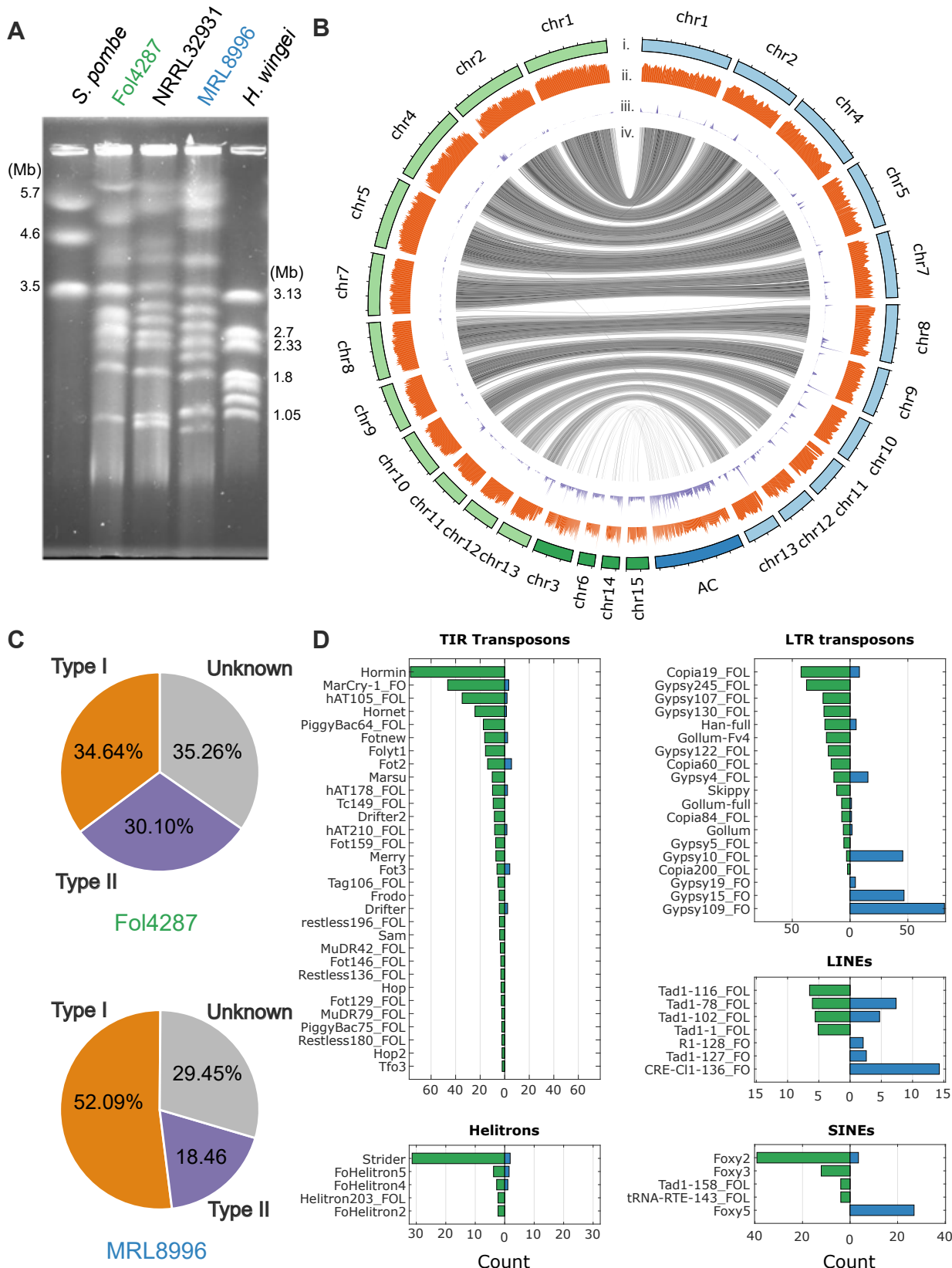
A
S. pombe
Fol4287
NRRL32931
MRL8996
H. wingei
(Mb)
5.7
4.6
3.5
(Mb)
3.13
2.7
2.33
1.8
1.05
B
i.
ii.
iii.
iv.
chr1
chr2
chr4
chr5
chr7
chr8
chr9
chr10
chr11
chr12
chr13
chr3
chr6
chr14
chr15
AC
C
Type I
Unknown
34.64%
35.26%
30.10%
Type II
Fol4287
Type I
Unknown
52.09%
29.45%
18.46
Type II
MRL8996
D
TIR Transposons
Hormin
MarCry-1_FO
hAT105_FOL
Hornet
PiggyBac64_FOL
Fotnew
Folyt1
Fot2
Marsu
hAT178_FOL
Tc149_FOL
Drifter2
hAT210_FOL
Fot159_FOL
Merry
Fot3
Tag106_FOL
Frodo
Drifter
restless196_FOL
Sam
MuDR42_FOL
Fot146_FOL
Restless136_FOL
Hop
Fot129_FOL
MuDR79_FOL
PiggyBac75_FOL
Restless180_FOL
Hop2
Tfo3
60 40 20 0 20 40 60
LTR transposons
Copia19_FOL
Gypsy245_FOL
Gypsy107_FOL
Gypsy130_FOL
Han-full
Gollum-Fv4
Gypsy122_FOL
Copia60_FOL
Gypsy4_FOL
Skippy
Gollum-full
Copia84_FOL
Gollum
Gypsy5_FOL
Gypsy10_FOL
Copia200_FOL
Gypsy19_FO
Gypsy15_FO
Gypsy109_FO
50 0 50
LINEs
Tad1-116_FOL
Tad1-78_FOL
Tad1-102_FOL
Tad1-1_FOL
R1-128_FO
Tad1-127_FO
CRE-Cl1-136_FO
15 10 5 0 5 10 15
Helitrons
Strider
FoHelitron5
FoHelitron4
Helitron203_FOL
FoHelitron2
30 20 10 0 10 20 30
Count
SINEs
Foxy2
Foxy3
Tad1-158_FOL
tRNA-RTE-143_FOL
Foxy5
40 20 0 20 40
Count

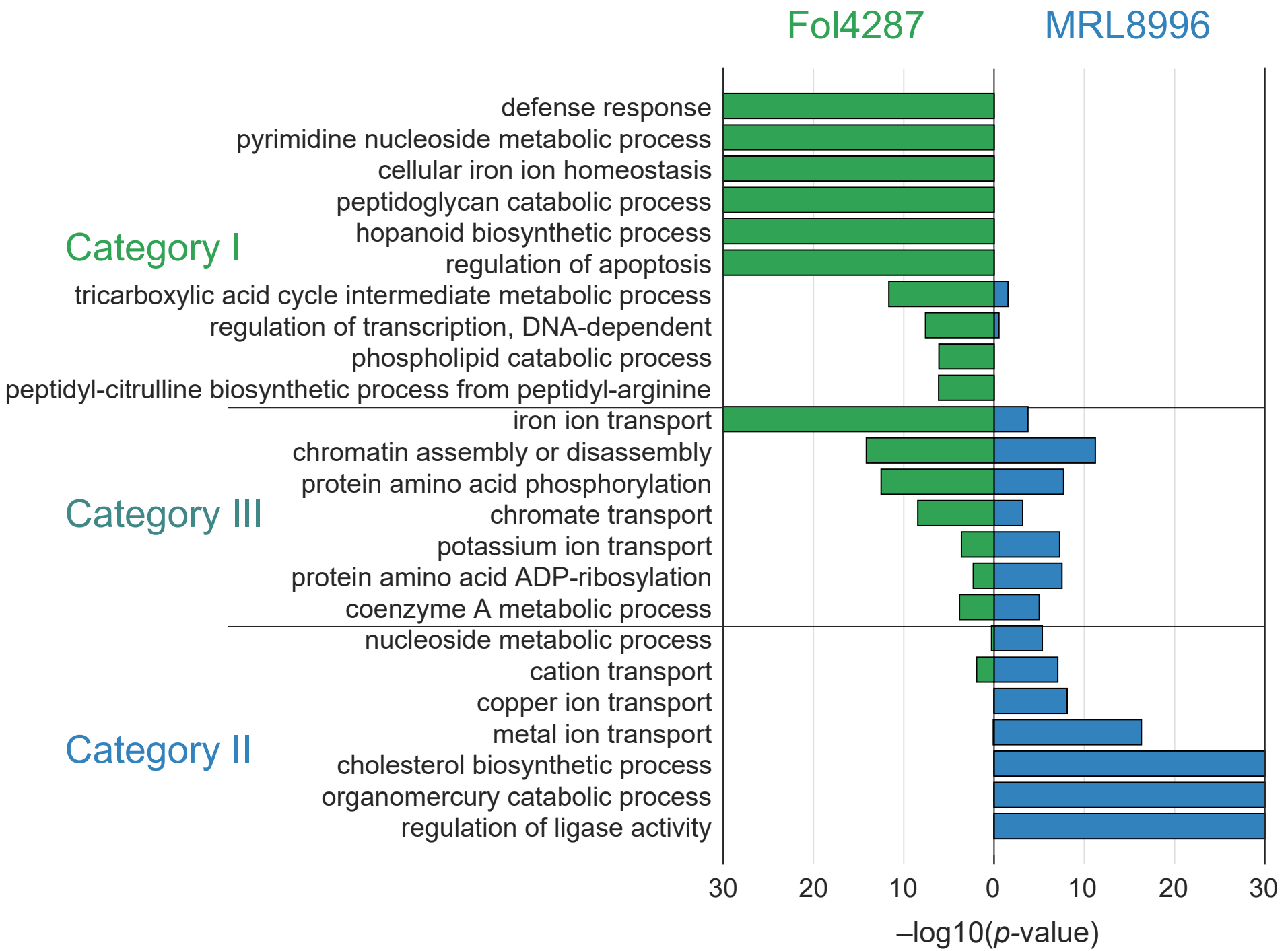
Fol4287
MRL8996
Category I
defense response
pyrimidine nucleoside metabolic process
cellular iron ion homeostasis
peptidoglycan catabolic process
hopanoid biosynthetic process
regulation of apoptosis
tricarboxylic acid cycle intermediate metabolic process
regulation of transcription, DNA-dependent
phospholipid catabolic process
peptidyl-citrulline biosynthetic process from peptidyl-arginine
Category III
iron ion transport
chromatin assembly or disassembly
protein amino acid phosphorylation
chromate transport
potassium ion transport
protein amino acid ADP-ribosylation
coenzyme A metabolic process
Category II
nucleoside metabolic process
cation transport
copper ion transport
metal ion transport
cholesterol biosynthetic process
organomercury catabolic process
regulation of ligase activity
30
20
10
0
10
20
30
–log10(p-value)